Chelation, formulation, encapsulation, retention, and in vivo biodistribution of hydrophobic nanoparticles labelled with 57Co-porphyrin: Oleylamine ensures stable chelation of cobalt in nanoparticles that accumulate in tumors

Pablo Hervella, Johan HygumDam, Helge Thisgaard, Christina Baun, Birgitte Brinkmann Olsen, Poul Flemming Høilund-Carlsen, David Needham

PII: S0168-3659(18)30567-4
DOI: doi:10.1016/j.jconrel.2018.09.027
Reference: COREL 9479

To appear in: *Journal of Controlled Release*

Received date: 24 September 2018
Accepted date: 30 September 2018

Please cite this article as: Pablo Hervella, Johan HygumDam, Helge Thisgaard, Christina Baun, Birgitte Brinkmann Olsen, Poul Flemming Høilund-Carlsen, David Needham , Chelation, formulation, encapsulation, retention, and in vivo biodistribution of hydrophobic nanoparticles labelled with 57Co-porphyrin: Oleylamine ensures stable chelation of cobalt in nanoparticles that accumulate in tumors. Corel (2018), doi:10.1016/j.jconrel.2018.09.027

Chelation, formulation, encapsulation, retention, and *in vivo* biodistribution of hydrophobic nanoparticles labelled with ^{57}Co-porphyrin: Oleylamine ensures stable chelation of cobalt in nanoparticles that accumulate in tumors.

Pablo Hervella*[1,2], Johan HygumDam[3], HelgeThisgaard[3], Christina Baun[3], Birgitte Brinkmann Olsen[3], Poul Flemming Høilund-Carlsen[3], David Needham*[1, 4, 5].

1. Center for Single Particle Science and Engineering, (SPSE), Department of Physics, Chemistry and Pharmacy, University Southern Denmark, Campusvej 55, DK-5230, Odense, Denmark
2. Clinical Neurosciences Research Laboratory, Health Research Institute of Santiago de Compostela (IDIS), Travesa da Choupana s/n, 15706 Santiago de Compostela, Spain
3. Department of Nuclear Medicine, Odense University Hospital, Sdr. Boulevard 29, 5000, Odense C, Denmark
4. Department of Mechanical Engineering and Material Science, Duke University, Durham, NC 27708,USA
5. School of Pharmacy, University of Nottingham, Nottingham, NG7 2RD, UK

*corresponding authors: pablo.hervella.lorenzo@sergas.es; d.needham@duke.edu

Abstract

Background and Motivation

While small molecules can be used in cancer diagnosis there is a need for imageable diagnostic NanoParticles (NPs) that act as surrogates for the therapeutic NPs. Many NPs are composed of hydrophobic materials so the challenge is to formulate hydrophobic imaging agents. To develop individualized medical treatments based on NP, a first step should be the selection of patients who are likely responders to the treatment as judged by imaging tumor accumulation of NPs. This requires NPs with the same size and structure as the subsequent therapeutic NPs but labelled with a long-lived radionuclide. Cobalt isotopes are good candidates for NP labelling since ^{55}Co has half-life of 17.5h and positron energy of 570 keV while ^{57}Co ($t_{1/2}$ 271.6 d) is an isotope suited for preclinical single photon emission tomography (SPECT) to visualize biodistribution and pharmacokinetics of NPs. We used the hydrophobic octaethyl porphyrin (OEP) to chelate cobalt and to encapsulate it inside hydrophobic liquid NPs (LNPs). We hypothesized that at least two additional hydrophobic axial ligands (oleylamine, OA) must be provided to the OEP-Co complex in order to encapsulate and retain Co inside LNP.

Results

1. ***Cobalt chelation by OEP and OA:*** The association constant of cobalt to OEP was 2.49×10^5 M^{-1} and the formation of the hexacoordinate complex OEP-Co-4OA was measured by spectroscopy. **2**. ***NP formulation and characterization:*** LNPs were prepared by the fast ethanol injection method and were composed of a liquid core (triolein) surrounded by a lipid monolayer (DSPC:Cholesterol:DSPE-PEG_{2000}). The size of the LNPs loaded with the cobalt complex was 40 ± 5 nm, **3.** ***Encapsulation of OEP-Co-OA:*** The loading capacity of OEP-Co-OA in LNP was 5 mol%. **4**. ***Retention of OEP-^{57}Co-4OA complex in the LNPs:*** the positive effect of the OA ligands was demonstrated on the stability of the OEP-^{57}Co-4OA complex, providing a half-life for retention in PBS of 170 h (7 days) while in the absence of the axial OA ligands was only 22h. **5** ***Biodistribution Study:*** the *in vivo* biodistribution of LNP was studied in AR42J pancreatic tumor-bearing mice. The estimated half-life of LNPs in blood was about 7.2 h. Remarkably, the accumulation of LNPs in the tumor was as high as 9.4% ID/g 24 h

after injection with a doubling time for tumor accumulation of 3.22h. The most important result was that the nanoparticles could indeed accumulate in the AR42J tumors up to levels greater than those of other NPs previously measured in the same tumor model, and at about half the values reported for the molecular agent ^{57}Co-DOTATATE.

Conclusions

The additional hydrophobic chelator OA was indeed needed to obtain a stable octahedral OEP-Co-4OA. Cobalt was actually well-retained inside LNP in the OEP-Co-4OA complex. The method described in the present work for the core-labelling of LNPs with cobalt is now ready for labeling of NPs with ^{55}Co, or indeed other hexadentate radionuclides of interest for preclinical *in vivo* PET-imaging and radio-therapeutics.

Keywords: Hydrophobic Nanoparticles, porphyrin, cobalt, 57Co, Octaethyl Porphyrin, Nanoparticles, PET imaging, SPECT, encapsulation, Triolein, PEGylation, Drug Release, tumor uptake, biodistribution.

Introduction

In a series of preclinical anti-cancer studies we have recently shown *in vitro* that a new Niclosamide Stearate (NS) prodrug NanoParticle (NSNP) are taken up by breast and prostate cancer cells, and are very effective at reducing cell viability and inducing cancer cell kill [1-4]. *In vivo* NSNP positively affects tumor growth delay in a breast cancer flank tumor [5] and metastatic spread in an osteosarcoma model of lung metastasis [5]. Interestingly, these studies have revealed new mechanisms of action for the "stealthy" prodrug nanoparticles. The new mechanisms are related to their kinetics of enzymolysis, their *in vivo* biodistribution and tumor-accumulation, as well their route of intracellular uptake and transport. An essential part of understanding the mechanisms of action for this, (and indeed any), i.v.-injected anti-cancer nanoparticle is to have a clear and quantitative measure of the blood circulation half-life and rate and extent of its accumulation in the perivascular space of the tumor interstitium. The overall goal of this study was to design, develop, and test a new method to formulate hydrophobic Liquid Nano-Particles (LNP) so that they can contain the hydrophilic radio-diagnostic cobalt ion. The clinical requirement is that they are small enough (<40 nm diameter, and preferably 20nm – 25nm) such that they can potentially extravasate into the tumor interstitium of human tumors. Tested here in implanted AR42J pancreatic tumor–bearing mice, we explored the possibility that they can report on the vascular permeability and the potential Enhanced Permeability and Retention (EPR) effect for subsequent studies of similar-sized therapeutic NPs containing anti-cancer drugs [6, 7].

Clearly, EPR is a relative-size issue. *Is the vasculature of each tumor permeable enough to allow each type of nanoparticle to extravasate?* A recent comprehensive 10-year review by Wilhelm, et al [8], revealed that, on average, only 0.7% of the administered nanoparticle dose is found to be delivered to a solid tumor. Also, there is now an emerging recognition that the cut-off in NP size for passage through human tumor vasculature is probably much less than the value usually assumed from subcutaneous-implants in animal studies of 500 nm-1μm [9]. Thus, it seems that some tumors are quite permeable, (especially implanted animal tumors used in preclinical studies), and so most nanoparticles can extravasate; while other tumors, perhaps especially in humans, are relatively impermeable, and so nanoparticles are excluded from the tumor interstitium and consequently have limited efficacy. For example, a trial by O'Brien in 2004 for *metastatic breast cancer* [10] showed that Doxil (Pegylated Liposomal Doxorubicin) was no better than free drug alone. That is, even though Doxorubicin has a

half-life of only 2 min, and Doxil has a half-life of 73.9 h: *"the overall survival (OS), was comparable with both treatments." "OS median Doxil, 21 months versus doxorubicin, 22 months).* Doxil was tested [11] and later approved for ovarian cancer in 2005, but again, with little therapeutic benefit. When compared to topotecan, the time to progression for Doxil was 4.1 months; topotecan - 4.2 months; overall median survival for Doxil was 14.4 months; topotecan 13.7 months; and the overall tumor response rates were 19.7% (47 patients) in the Doxil arm, and 17% (40 patients) in the topotecan arm. Compared to topotecan then, improvement in time-to-progression for Doxil was 0.1 months, which is only a 2.4% PFS. So why was Doxil so inefficient in these human cancers?

Tumor accumulation of Doxil has only been measured in 15 human patients by SPECT [12] and, in the 4 breast cancers studied the % injected dose that had accumulated in the tumors at 72h was only 0.5% (5.3 ± 2.6% ID/kg) of that initially injected. So, while there still maybe problems associated with limited drug release, is Doxil, measured at 87.3 ± 8.5 nm diameter [13], just too big to extravasate into ovarian and metastatic breast tumors in humans and provide the needed amount of drug to achieve efficacy?

In our opinion, it is this problem of making sure we all use well-characterized animal models in terms of their vascular permeability and nanoparticles capable of extravasating that is at the crux of whether nanomedicines will ever be successful. And these characteristics need to be established in the clinic with human cancer patients. It is this preclinical and clinical need that has motivated our efforts to provide a radioactive-ion-labelled hydrophobic nanoparticle capable of extravasating into the tumor interstitium and qualifying tumors as permeable or not, informing the "go, no-go" decisions for subsequent nanomedicine therapy.

Molecular Diagnostics, Theranostics, and Diapeutics

While small molecules such as ^{18}F-Fluodeoxy glucose (^{18}F-FDG) [14, 15] and ^{11}C (acetate) [16] can be effectively used in cancer diagnosis, they do not necessarily provide detailed information about uptake and accumulation of drugs formulated as NPs. Thus, there is a well-established need in the nanomedicine community for imageable diagnostic NPs that act as surrogates for the drug-nanoparticles.

One approach is the *theranostic* nanoparticle. As reviewed by Xie et al [17] and others [18, 19] the field of theranostics aims to *"develop more specific, individualized therapies for various diseases, and to combine diagnostic and therapeutic capabilities into a single agent".*

In this paper we focus on the idea that diagnostics needs to come first and actually inform therapeutic intervention. And so we are developing two agents that are expected to behave similarly when administered *i.v.,* in terms of blood circulation and tumor accumulation in diagnosing and treating cancer. We therefore introduce the term, ***"Diapeutics"*** as a clinical-administration-sequence of 1) a diagnostic nanoparticle that will inform the clinician of the potential for nanomedicine intervention by 2) a subsequent nanoparticle containing the appropriate drug. As presented previously [7], our bottom-up- and endogenous-inspired design for therapeutic NPs requires them to be of a similar material and similar size to the natural LDL. Thus, underlying this concept, specifically for cancer, is the recognition that rapidly growing cancer cells have high numbers of LDLRs [20], some 4-100x greater than for normal cells. Numerous malignancies are known to over-express LDLR including brain, colon, prostate, adrenal, breast, lung, leukemia, sarcomas, and kidney tumors. As a result, cancers are known to take in more LDLs than normal cells, and in patients with cancer, their LDL count can even go down. An abundance of LDL receptor is also a prognostic indicator of metastatic potential, and the propensity to accumulate and store cholesteryl-ester is a sign of the aggressiveness of a patient's cancer [20]. Since LDLs are taken up by tumors [21] to aid their rapid cell-doubling and growth, the assumption is that, by definition, a size of 20-40 nm NP diameter is a critical parameter for promoting NP extravasation across the tumor vascular endothelium, such that, even without receptor-ligand targeting [7] the stealth NPs can then be taken up by the tumor cells in, at least, the perivascular space for therapeutic effects [5, 22].

Thus, like *"theranostic nanomedicine"* we take advantage of the high capacity of nanoparticles to perform both imaging and therapeutic functions, but prefer to separate the two functions into two ostensibly identical *"diapeutic"* nanoparticles. In the clinical situation then, the clinician needs to be informed if the nanoparticle cannot access the tumor interstitium, and if not, the therapeutic nanoparticle will be relatively useless in terms of tumor targeting. It is this concept then that has driven the research design for these studies. Further discussion of these ideas and their application in a specific "Individualized Medicine" example are given in Discussion.

The need for hydrophobic liquid NPs for PET imaging

Not surprisingly given the need for anticancer drugs to act intracellularly on often membrane-bound protein targets [23], many of the drugs that are effective in cancer are relatively hydrophobic [24]. They are characterized as having high lipophilicity and low water-solubility and therefore low permeability (low absorption in humans) when taken orally [25]. They are classified in the Biopharmaceutics Classification System (BCS) [26] as BCS Class IV - Low Permeability, Low Solubility. In fact it is recognized that approximately 90% of pipeline drugs fall into the two low solubility categories of BCS II & IV [27]. This lack of good aqueous solubility is a key obstacle in the development and clinical use of these anticancer compounds including repurposed drugs (such as niclosamide) and newly developed small-molecule anticancer compounds, where the use of a simple oral formulation often fails to elicit biological potency and/or provides sufficient exposure to even validate the drugs.

Consequently, in an attempt to solve this problem in the development of such highly notorious BCS class IV drugs [25] researchers have turned to more advanced formulations. Many of the NPs currently being tested and developed in nanomedicine for drug delivery are, by necessity, composed of hydrophobic-cored materials. In contract many of the imaging agents are ions, and so are very soluble in water and do not partition into low dielectric hydrophobic environments. The challenge then in making a diagnostic nanoparticle that matches the therapeutic nanoparticle is to formulate oil-soluble hydrophobic imaging agents.

In a recent paper [28], we introduced a new approach to label the core of hydrophobic liquid NPs (LNPs) composed of glyceryl trioleate (triolein, TO) with water-soluble copper using the hydrophobic chelator octaethyl porphyrin (OEP). We demonstrated that a hydrophilic ion such as Cu^{2+} could be well-encapsulated and retained within the low dielectric core of the LNP. The goal of this earlier study was to create such a particle with a diameter and surface structure similar to a subsequent therapeutic NP that would contain a hydrophobic drug. As outlined above, the eventual application of the developed LNP is in tumor diagnostics, requiring a particle that can measure the nanoparticle half-life in the blood stream and can take advantage of, and indeed demonstrate, the permeability of the tumor vasculature to NPs, indicating the likely tumor accumulation of subsequent anti-cancer NPs. When used as a non-invasive analysis of the body distribution of such nanocarriers, the NP is expected to be a useful tool for preclinical as well as clinical development of NPs and indeed new and existing nanomedicines.

While the encapsulation principle was demonstrated for copper ions by Hervella et al [28], there is a need to extend these approaches to other ions of interest that could bring NP diagnostics and therapeutics to the clinic. One limitation of OEP used as the chelator is that, due to the number of donor sites in the porphyrin ring (four), the coordination number of the final porphyrin-radionuclide complex is correspondingly only four. This coordination number is enough to chelate soft metals such as Cu [29], but it is a limitation to stably chelate harder metals of interest, like, for example, ^{89}Zr, ^{86}Y,^{57}Co,^{58m}Co,or ^{55}Co [30]. The cobalt ion has a preferential coordination number of six and so has an octahedral geometry in metalloporphyrins [31]. It was therefore likely to not be as stably complexed by OEP and encapsulated in LNP as the four-coordinated copper and a preferential square planar structure in metalloporphyrins [31]. In other porphyrin-cobalt systems, the demand of axial ligands has been supplied by the solvent [32] or, in the case of vitamin B12, by a cyanide and an adenosine group [33], all of them with high water solubility. Since the OEP-Co complex is aimed to be encapsulated inside the hydrophobic core of the LNP, we hypothesized that not only do we have to use a hydrophobic chelator, such as OEP, we have also to provide additional hydrophobic axial ligands to the OEP-Co complex in order to encapsulate cobalt inside the LNP. To this end, oleylamine (OA) was selected due to its hydrophobic properties (log P: 7.9; S_w: 0.15 μM) and to the well-known capacity of its amines to coordinate cobalt porphyrins [34]. We therefore expected that the stability of the six coordinated OEP-Co-OA complex would be better retained in LNPs compared with the four-coordinated OEP-Co. In this study then, we continued the work initiated with LNPs labelled with copper, but now including cobalt as the element that can be used to measure the biodistribution of the NP and actual concentrations of the LNP in tumors preclinically with either ^{57}Co and single photon emission tomography (SPECT) or ^{55}Co and positron emission tomography (PET).

Cobalt as a radionuclide of interest for molecule labeling

Isotopes of cobalt provide several interesting properties in diagnostics and radiotherapy. ^{55}Co is an isotope of interest for PET imaging with long-circulating molecules and macromolecules due to its long half-life ($t_{½}$) of 17.5h and its average positron energy of 570 keV [35]. ^{57}Co ($t_{1/2}$ 271.6 days, Eγ=122 keV (86%), 136 keV (10%)), is a SPECT isotope that is useful for preclinical studies to visualize biodistribution and pharmacokinetics of NPs [36] and also for protocol optimizations as a longer-lived gamma-emitting surrogate to ^{55}Co [37, 38].^{58m}Co is an Auger-electron emitting isotope with potentially

unique therapeutic applications [39, 40]. In the formulation studied here, we used ^{57}Co as the initial test ion and measured the ex-vivo biodistribution of LNPs.

Biodistribution studies based on cobalt have been reported for peptides [38-42], including high contrast PET-imaging of gastrin releasing peptide receptor expression in prostate cancer using the cobalt-labeled bombesin antagonist RM26 [43], affibodies [37, 44, 45], vitamin B13 (Schiling test)[46], lymphocytes [47] and even for therapeutic drugs (Bleomycin formulated inside liposomes [36]). All these studies show the feasibility of using cobalt as an imaging agent for molecules with long half-lives in the bloodstream, suggesting that cobalt is a good candidate for the study of the biodistribution profile of NPs and their tumor accumulation.

NP labeling using long-lived radioisotopes

In preclinical studies, the *in vivo* imaging of NPs by PET has been carried out almost exclusively using ^{64}Cu as the contrast agent [48-53], hence, our initial interest in encapsulating copper [28]. In the above-referenced ^{64}Cu studies, the particles were labelled by using a water-soluble chelator (usually DOTA) that is attached to the particle surface. While this method allowed the efficient labelling of the NPs surface, it showed *in vivo* instability due to trans-chelation reactions in the liver [54-57]. In order to overcome this important drawback, we have therefore developed new techniques to label the core of LNPs [28] rather than the surface. Previous efforts by others include polymer NPs with ^{64}Cu-DOTA-acetylene core [58], liposomes with their aqueous core loaded with ^{64}Cu-DOTA [50], or porphyrin-based NPs labelled with a^{64}Cu-porphyrin phospholipid derivative [51]. Interestingly with respect to encapsulation and retention in the NP core, using the hydrophobic chelator OEP [28] we demonstrated that a hydrophilic ion such as Cu^{2+} could be encapsulated and retained within the low dielectric core of a hydrophobic NP, but only if the core was a liquid (as TO) compared to a solid core (as cholesteryl acetate), hence our preference for Liquid cored Nanoparticles (LNP).

The aim of the current work then was to label the core of similarly LNPs with the cobalt ion, recognizing that it requires hexadentate chelation. Surface-labeling is the most used strategy to label liposomes with radionuclides, since it can be done post NP formation by ligand attachment to preformed NPs. However, we now present a new example of the radionuclide-labeling for our NP achieved inside the core of the hydrophobic LNP. We modified the core-loading method used for copper ions [28] to successfully label NPs with cobalt ions by including OA. This new method is now

available alternative to surface chelators for labeling hydrophobic NPs for *in vivo* imaging, and we show here the principles underlying their encapsulation-stability and preclinical-utility.

Materials and methods

Materials

TO, OEP (2,3,7,8,12,13,17,18-Octaethyl 21*H*,23*H*-porphyrin), OA, and cobalt (II) chloride were purchased from Sigma-Aldrich. Carrier-free Co-57 (0.1 M HCl, 370 MBq) was purchased from Perkin-Elmer. Cholesterol, 1,2- Distearoyl-sn-glycero-3-phosphocholine (DSPC), and 1,2-distearoyl-sn-glycero-3-phosphor-ethanolamine-N-[amino(polyethyleneglycol)-2000] (DSPE-PEG^{2000}) were purchased from Avanti Lipids. Ethanol (99%) and chloroform were purchased from VWR. Human serum from human male AB plasma, sterile filtered, was purchased from Sigma. Other chemicals were purchased from Sigma-Aldrich. All reagents and solvents were used without further purification.

Safety/Toxicity

The chemical composition of the LNP was selected following the natural design of the endogenous LDL, and so the LNP are composed by phospholipids, cholesterol and triolein, materials that are widely used in drug delivery due to the lack of toxicity. These materials are Generally Regarded as Safe (GRAS) as reviewed by van Hoogevest and Wendel [59]. While Porphyrin-based compounds like OEP, can generate reactive singlet oxygen when activated by light, in the absence of light the porphyrin has very low toxicity, with an IC50 is in of 100 μM [60, 61]. Finally, for Cobalt isotopes, Jansen et al. [62] concluded that a safe dose for free ^{57}Co in humans would be 14.8 MBq. In this first preclinical study our injected dose was 62 ± 4 kBq per animal that was shown to be safe in terms of animal weights. Thus, it appears to be safely encapsulated in the nanoparticles, and so the human dose, if trialed, may actually be used at a higher dose than for free cobalt.

Methods

1. Cobalt chelation by OEP and OA

The main challenge was to stably incorporate a very hydrophilic Co^{2+} ion, (logP: 0.95, water solubility (S_w): 4 M) inside the hydrophobic TO core of the LNP. The strategy was to first chelate Co^{2+} with the

highly hydrophobic OEP (LogP 7.8, Sw: 16 µM), then complete the coordination of Co with the hydrophobic ligand OA (logP: 7.5; Sw: 0.15 µM) and finally encapsulate the resulting OEP-Co-OA complex inside the LNP.

OEP (25 nmol) and $CoCl_2$ (25 nmol) were dissolved in 1 mL of ethanol in a sealed glass vial, and the solution was placed in a microwave oven for 3 minutes at 850 W to produce the **OEP-Co** complex. After the solution was cooled down to room temperature, OA (100 nmol i.e., a mol ratio of 4:1 with OEP-Co, unless otherwise specified) was added to the solution and the resulting mixture was placed again in the microwave oven for another 1 min at 850 W (**Scheme 1**).The resulting **OEP-Co-OA** complex was then used without further purification.

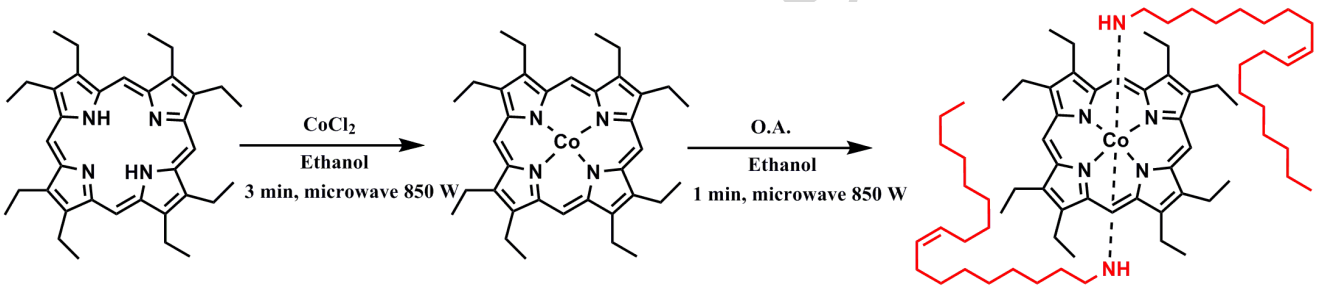

Scheme 1. ***Schematic representation of the chelation reaction***. 25 nmol Co^{2+} (as $CoCl_2$) was mixed with 25 nmol octaethylporphyrin (OEP) in ethanol and was exposed to 850W microwaves for 3 minutes. Then OEP-Co-OA was prepared by adding 100 nmol(mol ratio of 4:1 with OEP-Co and therefore a 2x excess) Oleyl Amine (OA) in the ethanolic solution of OEP-Co and exposed again to 850W microwaves for 1 minutes.

The chelation reaction was monitored by UV-Vis spectroscopy by following the spectral changes of OEP in the presence of different amounts of $CoCl_2$. The association constant was calculated by measuring the decrease in absorbance of OEP (5 nmol) in presence of different amounts of $CoCl_2$ (ranging from 0 to 5µM). The mixture was heated in a microwave for 3 min at 850W and the UV–Vis spectra were recorded in a Shimadzu UV-2600 spectrophotometer. All measurements were carried out in triplicate at 20 °C.

The chelation efficacy of ^{57}Co was evaluated by instant thin layer chromatography (TLC) using chromatography strips (Biodex), mounted with the 5 µL sample and eluted with 0.2 M citric acid (pH 2) and cut at the line. The radioactivity of both halves was measured in an Atomlab 950 well counter calibrated with Cs-137. Free cobalt eluted on top while OEP-^{57}Co-OA was retained at the bottom.

2. NP formulation and Characterization

Once cobalt was chelated by OEP or OEP plus OA, the complex was encapsulated inside LNP using the fast ethanol injection method, again developed previously for encapsulation of OEP-Cu [28]. Based on our previous studies [7, 28, 63] we selected TO as a model hydrophobic molecule, and solvent for the OEP-Co-OA complex, because of its high insolubility in water, and as a test particle that could be replaced in subsequent studies by hydrophobic drugs to create a potentially therapeutic LNP. Moreover, having already found that OEP was better retained in a liquid- than a solid-core [28, 63] efforts were made to create the smallest NP with this material and its encapsulated complexes. The components of the LNP and their physicochemical properties are listed in **Table 1**.

Table 1.Physical Properties of NP Materials. The lipids used to prepare Liquid NPs (LNP) were TO (TO), DSPC, Cholesterol and DSPEPEG. Octaethylporphyrin (OEP) and cobalt were encapsulated in this core. Oleyl Amine (OA) was used as a co-ligand. All water solubility and LogPs were obtained from ALOGPS (vclab.org).

Molecule	Molecular Weight	Melting Point	Water Solubility	LogP
Triolein	885 Da	-5.5°C	6.9 nM	10.8
DSPC	790 Da	55°C (Tm)	26 nM	5.9
Cholesterol	386 Da	148 °C	72 nM	7.0
DSPE-PEG^{2000}	2790 Da	12.8°C (Tm)	190 nM	2.9
$CoCl_2$	129 Da	735°C	4 M	0.95
OEP	535 Da	322°C	16 µM	7.8
OEP-Co	593 Da	-	21 µM	2.04
OA	267 Da	21 °C	0.15 µM	7.5
OEP-CO-OA	1124 Da	-	0.20µM	3.1

NPs were prepared using a modification of the solvent injection technique, named *fast ethanol injection* [28]. Briefly, all the components that form the NPs, TO (1 µmol), DSPC (0.45 µmol), Cholesterol (0.5 µmol) and DSPE-PEG^{2000} (0.05 µmol) and the Co complexes, OEP-Co or OEP-Co-OA (both at 25

nmol), were first dissolved in 1 mL ethanol. NPs were then made by using an automated syringe (eVOL XCHANGE, SGE analytical sciences) to inject the resulting 1 mL ethanol solution at a flow rate of 833 µL/s directly into 9 mL of deionized water, held in a 12 ml scintillation vial. Upon completion of mixing, the ethanol was removed by ultrafiltration (Amicon tubes, size cut-off 100.000 Da, 4000 rcf, 10 min). The sample was washed with deionized water 2 times, and again re-concentrated by removing the water by ultrafiltration. The final volume was adjusted to 10 mL to give a final particle suspension concentration of cobalt of 2.5 µM, and the particles were then used without further purification.

The size of the NPs and their polydispersity index (**P.I.**) were measured by Dynamic Light Scattering (**DLS**) in a Beckman Coulter DelsaMax Pro (laser power: 50mW, wavelength: 532 nm). The Z-potential was measured by Phase Analysis Light Scattering (PALS) in the same a Beckman Coulter DelsaMax Pro. The Z-potential measurements were carried out for LNP dispersed in Phosphate-Buffered Saline (PBS) keeping the NP concentration at 200µM. The UV-Vis spectra of the NPs were recorded in a Shimadzu UV-2600 spectrophotometer. All measurements were carried out in triplicates at 20 °C.

3. Encapsulation efficiency of OEP-Co-OA in LNP

3.1 Encapsulation efficiency of OEP-Co-OA in LNP

The encapsulation efficiency of OEP-Co-OA by NPs was first evaluated by fluorescence spectroscopy. This assay is based on the fluorescence of OEP-Co-OA that is only observed when the molecule is solubilized inside LNP, while it is totally quenched when dispersed in water. Encapsulation efficiency of OEP-Co-OA to NPs was measured by monitoring the fluorescent signal of LNP (200 µM) with increasing concentrations of OEP-Co-OA (0–10 mol%). The fluorescence spectra were recorded in an ISS Chronos Lifetime Spectrofluorometer, using an excitation wavelength of 400 nm. The emission was scanned over the range of 550–750 nm. Both the excitation and the emission slit widths were 1 nm. All measurements were carried out in triplicates at 20 °C.

3.2 Encapsulation efficiency of OEP-^{57}Co-OA in LNP

For the radioactive ion, ^{57}Co, the encapsulation efficiency of chelated OEP-^{57}Co and OEP-^{57}Co-OA inside NPs were evaluated by TLC. ^{57}Co (5.7 MBq) was chelated with 25 nmol OEP and then with

different amounts of OA. The LNP (200 µM) were then formulated with OEP-^{57}Co or OEP-^{57}Co-OA and the encapsulation efficiency was measured by TLC using chromatography strips (Biodex), mounted with 5 µL sample and eluted with 0.2 M citric acid (pH 2) and cut at the line. The radioactivity of both halves was measured in an Atomlab 950 well counter calibrated with Cs-137.The free ^{57}Co eluted to the top of the TLC strip while OEP-^{57}Co and OEP-^{57}Co-OA were retained in the NP and did not elute and so was measured at the bottom of the TLC strip as described above. All measurements were carried out in triplicate.

4. OEP-Co or OEP-Co-OA Retention and stability studies at 37°C

NP stability against aggregation and the retention of the radioisotope ^{57}Co inside LNP were clearly key requirements for successful *in vivo* studies. The LNP were designed and intended for subsequently delivery of ^{57}Co (or ^{55}Co) to the perivascular space of tumors. As mentioned above, it was recognized that there is likely to be an upper limit to the extravasation from blood circulation into the tumor interstitium by the EPR effect, and so it was necessary to check, as much as possible *in vitro*, that particle size remained unaltered in the presence of ionic media (PBS). Thus, the stability of OEP-Co-OA loaded NPs against any size change versus time was evaluated in PBS. Any loss of ^{57}Co was also evaluated in PBS as well as serum in order to ensure that the ^{57}Co loading was stably retained inside the LNP in these media.

4.1 Size stability in PBS

LNP loaded with OEP-Co or OEP-Co-OA were dispersed in PBS to a final LNP concentration of 200 µM (OEP-Co or OEP-Co-OA concentration was 2.5 µM). The samples were then placed at 37°C and the particle size was measured versus time during 24 h. The size of NPs and P.I. were measured by DLS in a Beckman Coulter DelsaMax Pro (laser power: 50mW, wavelength: 532 nm). All measurements were carried out in triplicate.

4.2 OEP-^{57}Co or OEP-^{57}Co-OA Labelling stability in PBS

NPs were prepared as described above and were loaded with either OEP-^{57}Co (2.5 µM OEP, 5.7 MBq) and OEP-^{57}Co-OA (2.5 µM OEP, 10 µM OA, 5.7 MBq). The NPs were dispersed in PBS (LNP concentration 200 µM) and incubated at 37°C for 24 h. LNP labelled with OEP-^{57}Co-OA were also incubated in human plasma at 37ºC for 24h. The encapsulation efficiency of the samples versus time

was measured by TLC as described above (see section, *3.2 Encapsulation efficiency of OEP-^{57}Co-OA in LNP*). All measurements were carried out in triplicate.

5. In vivo biodistribution study

The biodistribution studies for this LNP were designed to obtain a quantitative measure of the biodistribution profile and the pharmacokinetics of the nanoparticles. Principally, this study was to show if and to what extent the LNP were accumulated in tumors in order to pave the way for formulation design and testing of a subsequent therapeutic NPs. Following *i.v.* injection into AR42J tumor–bearing mice of the OEP-Co-OA loaded LNP, measurements included circulation half-life of the intact LNP in the blood stream and its accumulation in these implanted pancreatic tumors. Other important pharmacokinetic parameters assessed included any potential for accumulation by organs and tissues (kidneys, adrenals, stomach, small intestine, pancreas, lungs, heart), and especially those of the RES, the liver and the spleen.

OEP-^{57}Co-OA NPs were prepared for the *ex vivo* biodistribution study as described above (***2. NP formulation***) using a radioactivity of 64.8 MBq of $^{57}CoCl_2$ (~1.6 nmol) chelated with 25 nmol of OEP and 100 nmol of OA in 1 μmol of TO and1 μmol of phospholipids. After fabrication, the particles were suspended in PBS and filtered with a 0.45 μm sterile filter before injection via tail vein. Injections into the animals were made by diluting the stock suspension of LNP with PBS.

Animal Tumor Model

Male NOD-SCID mice (bred-in-house) 10-12 week old were anesthetized with 1-3% isoflurane in 100% oxygen and inoculated s.c. in the right flank with $1x10^6$ AR42J pancreatic tumor cells that had been prepared in 50 μL of medium containing matrigel (Sigma-Aldrich; ratio 1:1). The tumors were allowed to grow for 11-13 days until reaching a weight of between 16-342 mg. Studies of the biodistribution of OEP-^{57}Co-OA loaded LNP were performed by i.v. injection of 62±4 kBq of the tracer (represented by $2.7x10^{11}$ NPs in PBS) in the anesthetized mice. The mice (n=4in each group) were euthanized and dissected 1h, 4h and 24h after NP injection. Organs were collected and weighed, and radio activities were measured with a 2470 Wizard Automatic γ Counter. Organ tracer activity distributions were determined as the percentage of injected activity per gram of tissue. All animal experiments were approved by *The Animal Experiments Inspectorate in Denmark, (approval number,* 2016−15−0201−01027).

Results

Following the work on copper ions encapsulated inside the core of hydrophobic LNP [28], we now present the results of a comprehensive study of the steps of optimization that were carried out for cobalt to: **1.** Chelate the cobalt; **2.** Formulate the LNP; **3.** Encapsulate chelated Co^{2+} ions in the LNP core; **4.** Measure how well the cobalt was retained in the NPs; and **5.** Measure the NP biodistribution *in vivo*, including tumor accumulation in tumor-bearing mice. Note: we used non-radioactive ^{59}Co for developing all the chelation, encapsulation, and retention studies, and switched to ^{57}Co for the *in vivo* biodistribution and tumor accumulation studies.

1. Cobalt chelation

1.1 Cobalt Chelation by OEP

Non-radioactive ^{59}Co was first chelated by the hydrophobic OEP to test its suitability for encapsulation into the hydrophobic LNP.

Association constant of Co to OEP

The association constant of cobalt to OEP was measured by recording the UV-Vis spectra of OEP (25μM) after chelation with different amounts of $CoCl_2$. As can be seen in **Figure 1A**, the absorbance of the Søret band of OEP (395 nm) decreased when OEP was chelated with different concentrations of $CoCl_2$ ranging from 0 to 50 μM. In tandem, a new peak at 411 nm increased in absorbance with increasing concentrations of cobalt. This new peak is attributed to the formation of the OEP-Co complex; its absorbance reached a maximum at the expected 1:1 mol ratio of OEP and cobalt, i.e., at 25μM $CoCl_2$ and 25μM OEP (dotted line in **Figure 1A**). The decrease in the Søret band of OEP (395 nm) with increasing concentration of cobalt was then used to measure the association constant of Co to OEP following a Benesi-Hildebrand plot [64]. **Figure 1B** shows the fit of the experimental data to the Benesi-Hildebrand plot defined by equation 1:

$$\frac{1}{\Delta A_{obs}^{395}} = \frac{1}{S\Delta\varepsilon K_{OEP-Co}[Co]} + \frac{1}{S\Delta\varepsilon} \qquad \textbf{eq. 1}$$

Where: ΔA_{obs}^{395} is the change in absorbance at 395 nm; S is the total concentration of OEP (5 μM); [Co]is the concentration of cobalt (0-5 μM); Δε the change in molar absorptivities of OEP and OEP-Co at 395

nm; and $K_{OEP\text{-}Co}$ is the association constant of Co to OEP. $K_{OEP\text{-}Co}$ was calculated from the ratio between the intercept and the slope resulting in a value of (2.49 ± 0.2) x10^5 M^{-1}, and was in the same range as we had measured earlier for OEP-Cu (5.44 x10^5 M^{-1}) [28].

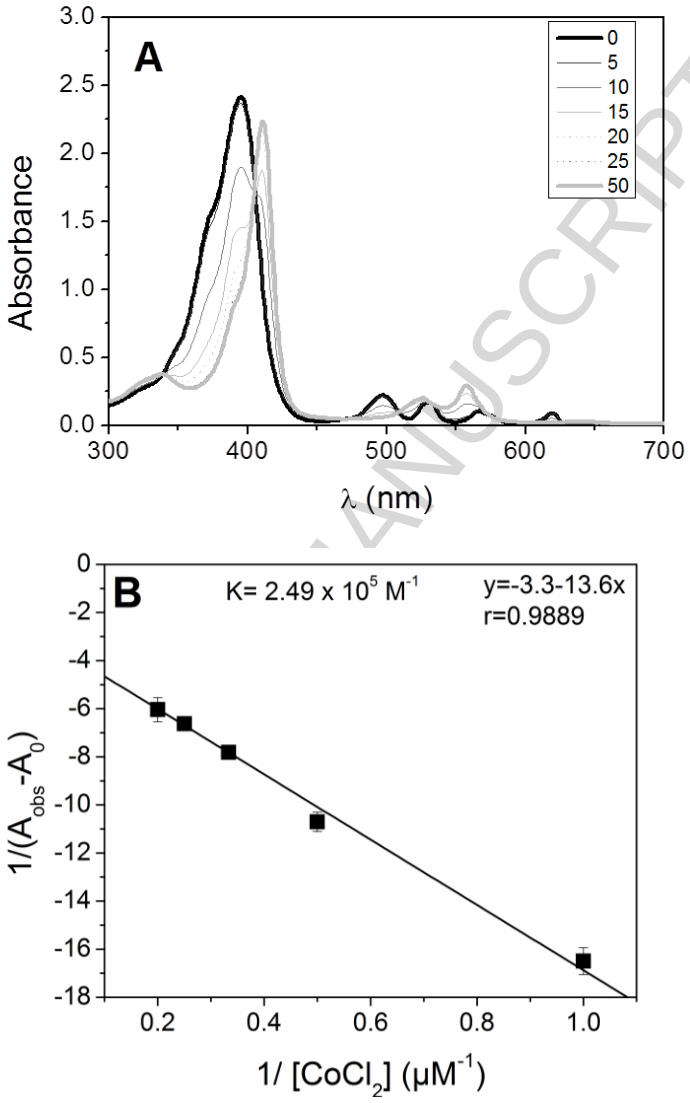

Figure 1.Cobalt chelation by OEP. A) UV-Vis spectra of OEP in ethanol (25µM) (black line) and OEP chelated with different concentrations of $CoCl_2$ ranging from 5 to 50 µM (grey lines). The Søret band is shifted from 395 nm for OEP (black line) to 411 nm for OEP-Co (grey line).All the spectra were measured in ethanol at a concentration of OEP of 25 µMB. **B)** Benesi-Hildebrand plot for the variation of the absorbance at 395 nm of OEP dissolved in ethanol (5 µM) with the concentration of $CoCl_2$ (ranging from 0 to 5 µM). The association constant of Co to OEP of 2.49x10^5 $M^{-1}$was calculated from the ratio between the intercept and the slope of the linear fit. All measurements were recorded in triplicate in ethanol at 20°C.

1.2 OEP-Co coordination by OA

We evaluated the number of moles of the hydrophobic ligand OA required to chelate the OEP-Co. The change in the coordination number of Co inside OEP-Co from 4 to 6, using OA as the axial ligand of OEP-Co, was monitored by UV-Vis spectra. While it was expected that the molecular-equivalent would be 2 per OEP-Co, we explored increasing amounts of OA in the coordination reaction with OEP-Co ranging from 12.5 µM (0.5 equivalents of OA in relation to OEP-Co) to 400 µM (16 equivalents of OA in relation to OEP-Co). The results are shown in **Figure 2**.

Since cobalt was chelated with OEP in ethanol, initially we tested the effect of OA on the OEP-Co coordination in this solvent (**Figure 2A**). However, ethanol itself adds two axial ligands to the planar structure of OEP-Co [65], thereby interfering with the OA donation. Thus, in ethanol, the UV-Vis spectra of OEP-Co in the absence of OA had a Søret band centered at 411 nm that was only slightly red-shifted to 413 nm in the presence of 1 equivalent of OA (25µM). Coordination with higher amounts of OA did not result in any change in the UV-Vis spectra, even at high OA concentrations of 400 µM (16 equivalents of OA).

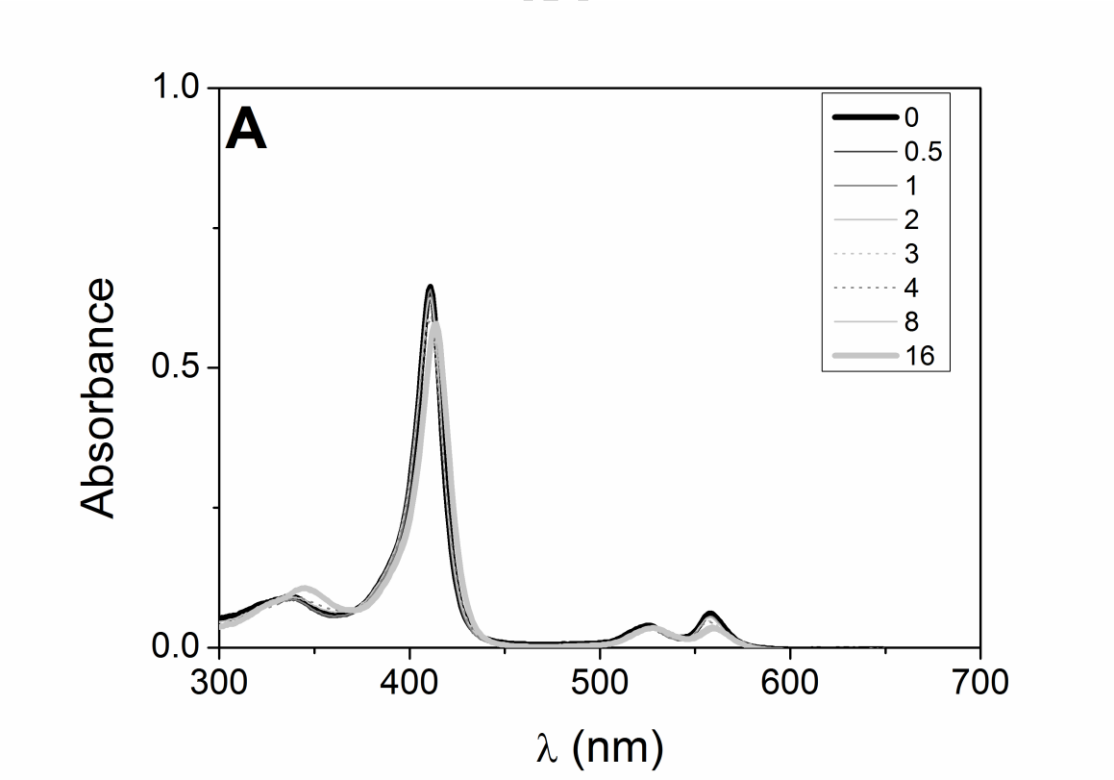

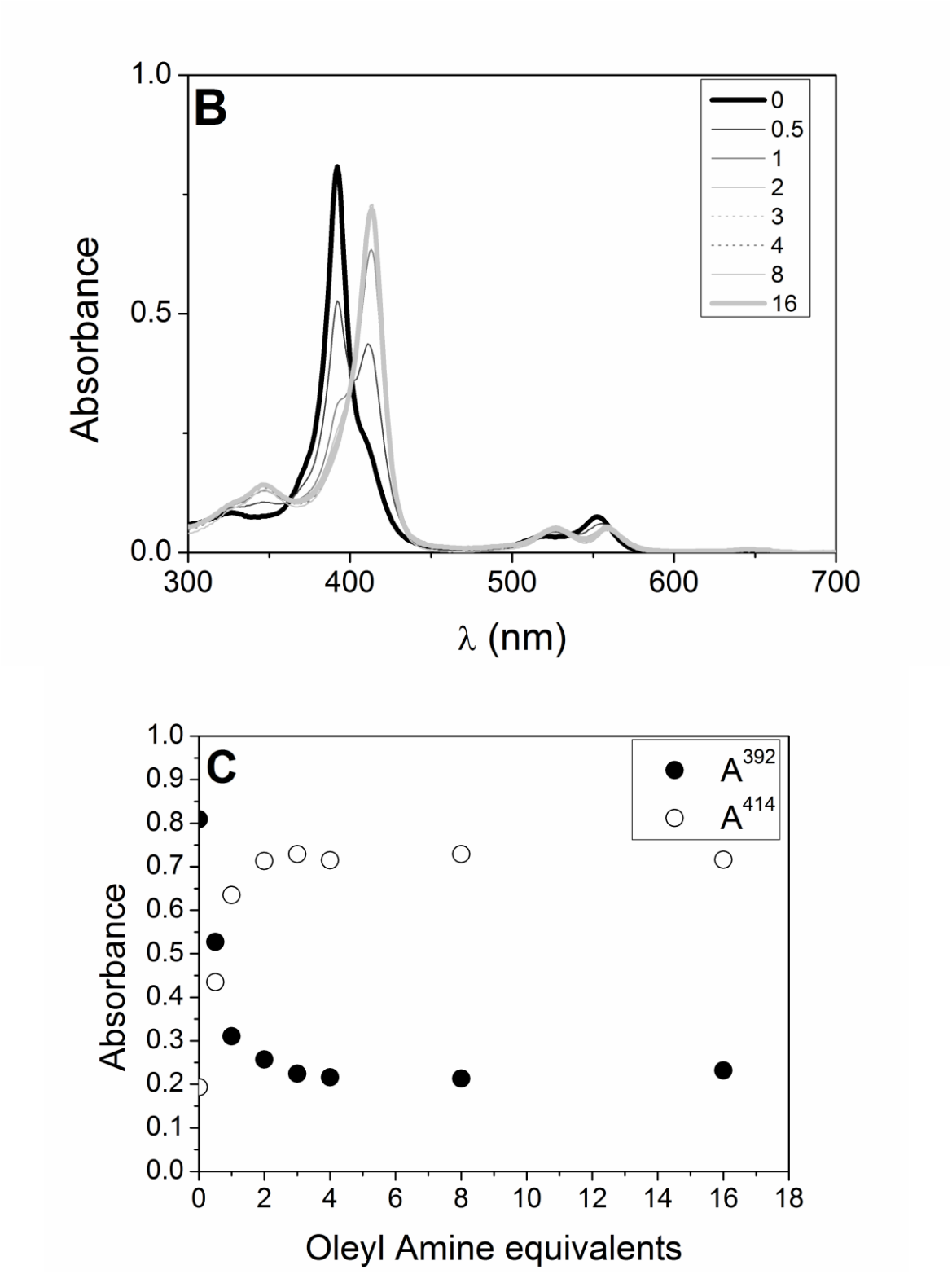

Figure 2.Coordination of OEP-Co by OA. A) UV-Vis spectra of OEP-Co in ethanol (5 µM) in the absence of OA (black line) and after coordination with different amounts of OA, from 0.5 equivalents (2.5 µM) to 16

equivalents (80 µM). The Søret band of OEP-Co and OEP-Co-OA was centered at 411 nm. Spectra were recorded in ethanol at 20°C. **B)**UV-Vis spectra of OEP-Co in chloroform (5 µM) in absence of OA (black line) and after coordination with different amounts of OA, from 0.5 equivalents (2.5 µM) to 16 equivalents (80 µM). The Søret band of OEP-Co (black line) was centered at 392 nm while is centered at 414 nm for OEP-Co-OA (grey line). Spectra were recorded in chloroform at 20°C. **C)** Plot of the Absorbance at 392 nm (black dots) and the absorbance at 414 nm (white dots) of OEP-Co dissolved in chloroform (5 µM) after being coordinated with different amounts of OA. A minimum value for the absorbance at 392 nm (OEP-Co) and a maximum value for the absorbance at 414 nm (OEP-Co-OA) were measured for OEP-Co coordinated with 4 equivalents of OA.

Obviously, ethanol is not a stable ligand in the LNP (it would rapidly dissolve out of the LNP when introduced into aqueous media), and so we had to choose a different solvent to measure the OA chelation. This solvent was chloroform that has a much lower donor number than ethanol (4 kcal mol^{-1}vs ethanol, which is 19.2 kcal mol^{-1}). Thus, a different and preferable behavior was observed when the complexes were dissolved in chloroform (**Figure 2B**). An intense blue-shift was observed for formation of the OEP-Co complex with this change in solvent, from 411 nm in ethanol to 393 nm in chloroform (the black lines in **Figures 2 A** and **B** respectively). No further blue-shift was observed for the OEP-Co-OA complex prepared with 2 or more equivalents of OA, and the Søret band of OEP (originally at 395 nm) was now measured at 414 nm. With this improved, less-interacting, solvent of chloroform, the addition of 0.5 and 1 equivalents of OA, gave two peaks that were observed in the UV-Vis spectra at 392 nm and 414 nm, indicating the co-existence of OEP-Co and OEP-Co-OA.

In order to optimize the amount of OA needed to fully chelate Co in the OEP-Co-OA complex, increasing amounts of OA equivalents were added and a plot of the absorbance at 392 nm (corresponding to the OEP-Co complex) and the absorbance at 414 nm (corresponding to OEP-Co-OA) vs the equivalents of OA was made. It can be seen from **Figure 2C**, that a minimum value for the absorbance at 392 nm and a maximum value for the absorbance at 414 nm were obtained at a concentration of OA of 4 equivalents (100 µM). Therefore the molar ratio 1:4 (for OEP-Co:OA) was selected for the next studies, hence now designated with the term OEP-Co-4OA.

2. Formulation and characterization of LNP

2.1 LNP formulation including the presence of OEP-Co-4OA

Influence of OA equivalents on size of LNP

All LNP were formulated using the same fast solvent injection method described in our previous paper [28]. Blank LNP, composed by TO (1 µmol), DSPC (0.45 µmol), cholesterol (0.5 µmol) and DSPE-PEG_{2000} (0.05 µmol), were prepared by this method. The diameter measured after the solvent injection was 28 ± 4 nm, with a P.I. of 0.27. This value is the cumulative average of the sample. The mass-weighted average shows a mean value of 22 ± 4 nm, while the number-weighted average was 20 ± 3 nm. After the sample was concentrated, each of the samples was dispersed in PBS and the diameter was measured again. The cumulative average diameters measured for each of the LNP was as follows: for blank LNP in PBS, the diameters were 33 ± 4 nm with a P.I. of 0.17; LNP labelled with 2.5 mol% of OEP-Co in PBS were 32 ± 3 nm, the same as blank LNP; LNP labelled with 2.5 mol% of OEP-Co plus the OA were also 32 ± 3 nm for 1eq of OA, but the diameter increased to 37.5 nm ± 3 nm for 2 eq of OA, and to 40 ± 5 nm for 4 and 8 equivalents of OA.

Thus, as shown in **Figure 3,** in contrast to the unlabeled and OEP-Co labelled LNP, coordination of OEP-Co with different amounts of OA (of 2, 3, 4 and 8 equivalents) resulted in a slight but significant increase ($p<0.05$) in the particle diameter especially with 4 and 8 equivalents of OA.

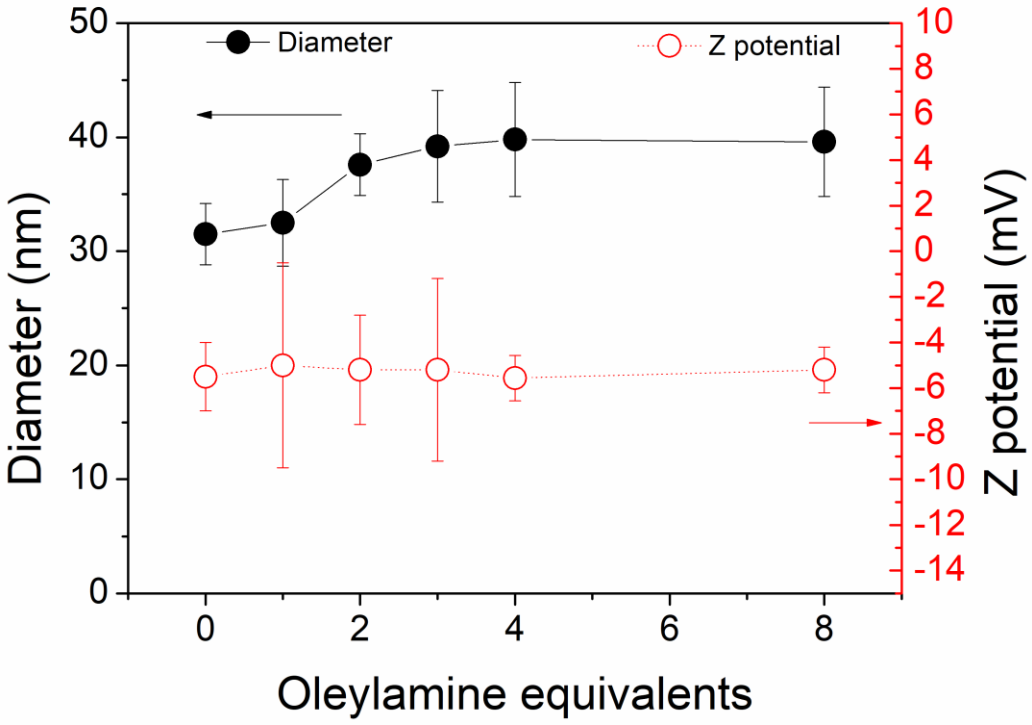

Figure 3. ***LNP Diameter and Z potential versus equivalents of OA.*** Comparison between the particle diameter vs the amount of OA for LNP loaded with OEP-Co coordinated with different concentrations of OA (0-8 equivalents). The final LNP concentration in PBS suspension was 200 µM for LNP (100 µM TO, 45 µM DSPC, 50 µM Cholesterol, 5 µM DSPEPEG). OEP-Co or OEP-Co-4OA concentration was 5 µM. All measurements were carried out in PBS at 20°C in triplicate.

All the above data is given in terms of the cumulative average size. Since we are attempting to make LDL-sized NPs (~20nm diameter [66]) for purposes of maximizing eventual *in vivo* EPR, it is important to understand the results in terms of what the DLS provides. The particle sizes measured by DLS were dependent on the mode employed for measurements. Thus, for completion, for each measurement mode, the average size of the sample prepared for the final injectable formulation of LNP, labelled with 2.5 mol% of OEP-Co plus 4 equivalents of OA, is shown in Supplemental Information **Figure S1**. Its intensity-weighted diameter was 51±5 nm, whereas the mass-weighted diameter was measured to be 40±5 nm, and the number-weighted diameter was 34±5 nm. Note, these diameters also include the PEG layer extending 3.5nm from the lipid head-groups [67], and so the core plus lipid monolayer would be diameter minus 7 nm. See later in Discussion, Scheme 2.

Regarding surface charge of the LNP, the results (also in **Figure 3**) showed that the Z-potential of LNP loaded with OEP-Co-OA was not dependent on the concentration of OA and a Z-potential value around -5.2 ± 3mV as measured for all NPs dispersed in PBS indicating that the OA was not surface active but bound inside the TO core as a cooperative ligand to the OEP-Co complexes as intended.

Establishing the required equivalents of OA for encapsulation of OEP-Co in NPs

Here, we first established the required equivalents of OA for encapsulation of OEP-Co in LNP at a single 2.5 μM concentration of OEP-Co and then varied the OA. The formulation of OEP-Co-OA prepared with different equivalent amounts of OA in OEP-Co loaded LNP was studied by UV-Vis spectroscopy. The results in **Figure 4A** show the differences in the UV-Vis spectra of LNP loaded with OEP-Co and OEP-Co-OA. As expected from the hydrophobic nature of the LNP core, it can be seen that the spectra of OEP-Co in LNP is similar to the spectra recorded in chloroform (**Figure 2B**). That is, in **Figure 4A**, in the absence of OA (i.e. just OEP-Co), the Søret band (black line) was centered at 392 nm while in the presence of OA (i.e. OEP-Co-OA) the Søret band (grey line) was centered at 414 nm. Interestingly, it should be noted that, for OEP-Co-OA loaded LNP prepared with 0.5 and 1 equivalents of OA, the Søret band was divided into two bands, suggesting the presence of both OEP-Co and OEP-Co-OA complexes.

The full conversion from OEP-Co to OEP-Co-OA is represented in **Figure 4B**, where the absorbance at 414 nm (maximum for OEP-Co-OA complexes) and the absorbance at 393 nm (maximum for OEP-Co complexes) are plotted vs the equivalents of OA. It can be seen that a maximum value for the absorbance at 414 nm is observed after 2 equivalents of OA. These results were in good agreement with the spectroscopic study carried out for the OEP-Co complex dissolved in chloroform (**Figure 2C**), where saturation was complete at 4 equivalents of OA. As we have shown previously [63], TO and chloroform are very close in terms of solvency for OEP complexes, i.e., the solubility limit of OEP in pure chloroform was 10 mM, and its solubility limit in pure TO was found to be very similar at 9.6 mM. However, since they are not exactly identical solvents, to be safe and sure, the OEP-Co-OA complex was encapsulated in LNP with 4 equivalents of OA. Thus, while only 2 equivalents would seem to be required to occupy the additional two valence of the octahedral coordination geometry of Co, and this spectrophotometric study confirmed this 1:2 coordination of OEP-Co with OA, we

actually used 4 equivalents of OA of in the OEP-Co-OA complex for *in vivo* testing, and so prepared it with the molar ratios of 1:1:4.

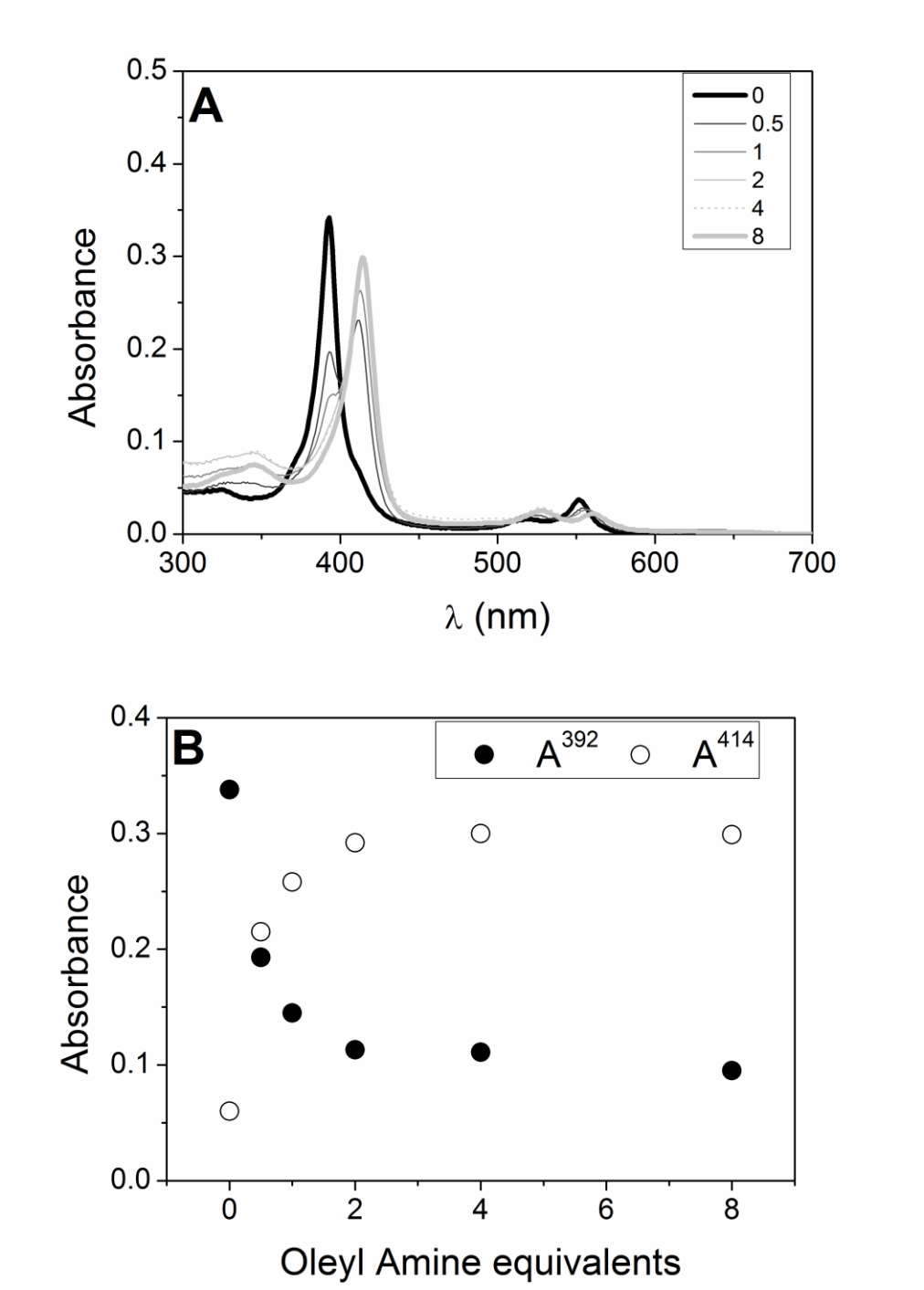

Figure 4.OEP-Co and OEP-Co-OA encapsulation in LNP: A) UV-Vis spectra of OEP-Co (2.5 µM) (black line) and OEP-Co-OA (2.5 µM grey line) encapsulated in LNP. OEP-Co-OA was prepared by the coordination of OEP-Co with different amounts of OA, from 0 equivalents to 8 equivalents (20 µM). The Søret band of OEP-Co loaded LNP (black line)

was centered at 392 nm and at 414 nm for OEP-Co-OA loaded LNP (grey line). LNP were composed by TO (100 μM), DSPC (45 μM), Cholesterol (50 μM) and DSPE-PEG_{2000} 5 μM) and were prepared by the fast ethanol injection method. Spectra were recorded in water at 20°C. **B)** Plot of the Absorbance at 392 nm (black dots) and the absorbance at 414 nm (opencircles) for OEP-Co encapsulated in LNP after being coordinated with different amounts of OA. A minimum value for the absorbance at 392 nm (OEP-Co) and a maximum value for the absorbance at 414 nm (OEP-Co-OA) were measured for OEP-Co coordinated with 2 equivalents of OA. LNP were composed by TO (100 μM), DSPC (45 μM), Cholesterol (50 μM) and DSPE-PEG_{2000} (5 μM) and were prepared by the fast ethanol injection method. OEP-Co or OEP-Co-OA concentration was 2.5 μM. Spectra were recorded in water at 20°C.

3. Influence of OEP-Co-4OA-loading on LNP size and maximum encapsulation of OEP-Co-4OA inside LNP

Having established the 1:1:4 coordination for OEP-Co-4OA at one loading-concentration (2.5 μM OEP-Co-4OA in 100 μM TO), we then evaluated the influence of the OEP-Co-4OA loading on the obtained diameter of the OEP-Co-4OA loaded LNP.

3.1 Influence of OEP-Co-4OA loading on LNP size

LNP were formulated with different amounts of OEP-Co-4OA, ranging from 0 to 10 mol% (0 – 10 μM) with respect to TO (100μM). The results are shown in **Figure 5**. The average size of blank LNP in PBS was 32 ± 3 nm. The size increased with increasing concentration of OEP-Co-4OA, until a diameter of 40 ± 5 nm was measured for LNP with an OEP-Co-4OA loading above 1.5mol%. As we have shown previously, OEP can also form crystalline material that could exist as their own NPs if not encapsulated [63]. Thus, as a control, the free OEP-Co-4OA complex in the absence of LNP was also formulated using the same solvent injection method. The average diameter of pure free OEP-Co-4OA NPs dispersed in PBS was 77 ± 11 nm.

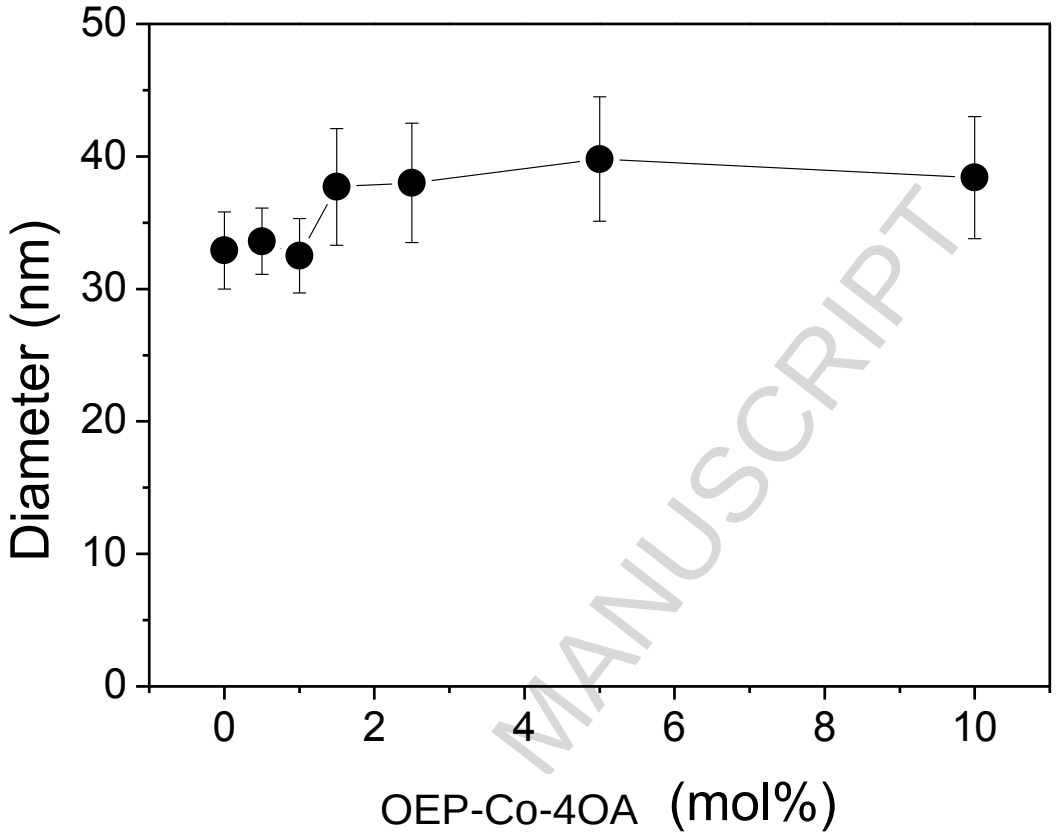

Figure 5. NP diameter versus molar concentration of OEP-Co-4OA. Comparison between the particle diameter vs OEP-Co-4OA concentration in LNP reported as mol% with respect to TO. OEP-Co-4OA was prepared with a 1:1:4 mol ratio. The final NP concentration in water suspension was 200 µM for LNP (100 µM TO, 45 µM DSPC, 50 µM Cholesterol, 5 µM DSPE-PEG). All measurements were carried out in water at 20°Cin triplicate.

Thus, the results obtained from the size measurements suggested that LNP showed a slight increase in average size when labelled with OEP-Co-4OA up to 2 and 4 mol% and that their size actually did not increase beyond that point.

3.2 Maximum Encapsulation of OEP-Co-4OA in LNP

We also determined the maximum amount of OEP-Co-4OA at this optimal ratio 1:1:4 that could be encapsulated in the LNP. The encapsulation of OEP-Co-4OA in LNP was evaluated by UV-Vis and fluorescent spectroscopy. The UV-Vis spectra of OEP-Co-4OA were recorded for LNP loaded with different amounts of OEP-Co-4OA, from 0 to 10 mol% (**Figure 6A**). We did not observe any change in the position of the Søret band that was measured at 414 nm independent of the concentration of OEP-

Co-4OA in the LNP. Also, the shape of the Søret band did not change with the concentration of OEP-Co-4OA, and it was the same as that for OEP-Co-4OA suspension in water (**Figure 6A**, insert).

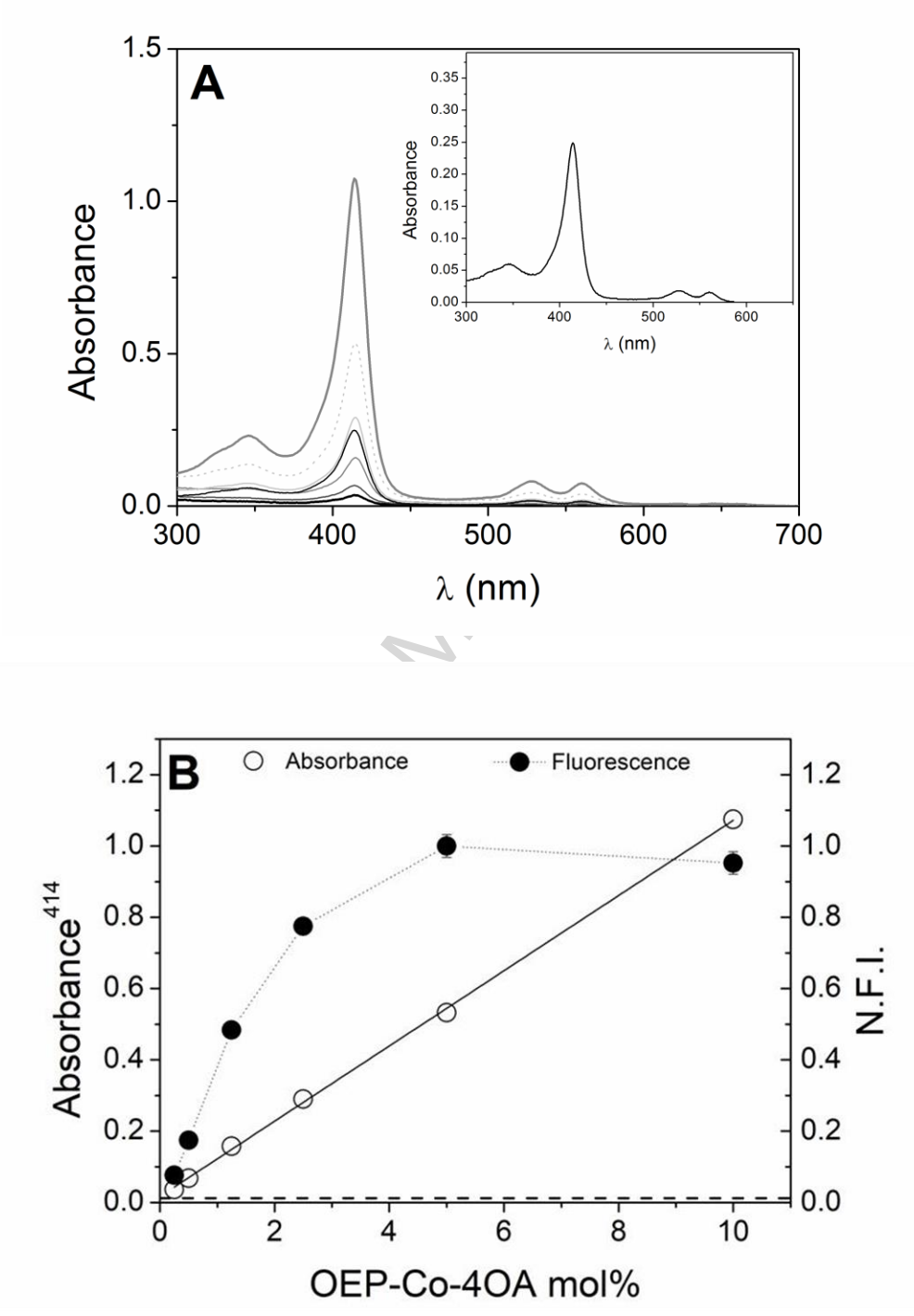

Figure 6.Maximum Encapsulation efficacy of OEP-Co-4OA in LNP.A) UV–Vis spectra of OEP-Co-4OA encapsulated in LNP. The concentration of LNP in water suspension was 200 µM for LNP (100 µM TO, 45 µM DSPC, 50 µM Cholesterol, 5 µM DSPE-PEG) and the concentration of OEP-Co-4OA ranged from 0.5 mol% to 10 mol%. All particles

were prepared by the fast solvent mixing technique and the UV-Vis spectra were recorded in water at 20°C. Insert: UV-Vis spectra of OEP-Co-4OA complex in water suspension (2.5 µM). The OEP-Co-4OA suspension was prepared by the fast solvent injection technique using the same conditions as for the LNP but without lipids. Of importance to note is that the Søret band is centered at 414 nm at all OEP-Co-4OA concentrations in LNP and also in suspension in absence of LNP. **B)** Plot of the absorbance at 414 nm (left hand axis) and the Normalized Fluorescence Intensity (N.F.I.) (right hand axis) vs the concentration of OEP-Co-4OA loaded into the LNP. The concentration of LNP in water suspension was 200 µM for LNP (100 µM TO, 45 µM DSPC, 50 µM Cholesterol, 5 µM DSPE-PEG) and the concentration of OEP-Co-4OA ranged from 0.5 mol% to 10 mol%. A linear fit is obtained for the absorbance at 414 nm vs the concentration of OEP-Co-4OA. The NFI was increased gradually and steeply with the concentration of OEP-Co-4OA to a maximum value obtained at 5 mol%. The fluorescence intensity of pure OEP-Co-4OA dispersed in water is represented by the dashed line. All particles were prepared by the fast solvent mixing technique and the UV-Vis spectra were recorded in water at 20°C.

In order to calculate the total concentration of OEP-Co-4OA in the LNP suspension a linear calibration plot was made of the absorbance at 414 nm (maximum for the Søret band of OEP-Co-4OA in hydrophobic environments) vs the concentration of OEP-Co-4OA (**Figure 6B**, open circles, left hand axis).

The encapsulation efficiency was then evaluated by fluorescence spectroscopy (**Figure 6B**). The fluorescent signal of OEP-Co-4OA dispersed in water was fully quenched giving no measureable fluorescent intensity for OEP-Co-4OA prepared in the absence of LNP. On the other hand, when OEP-Co-4OA was encapsulated in LNP, the fluorescent signal was recovered and the particles became fluorescent. This fact allowed for the quantification of the encapsulation of OEP-Co-4OA in LNP without using any separation technique. The fluorescent intensity was measured for OEP-Co-4OA in the range of 0-100 µM for LNP (100 µM), i.e., up to a 1:1 mol ratio. The results show that the fluorescence intensity gradually increased with increasing concentration of OEP-Co-4OA until a plateau was reached at 5 mol% concentration, which therefore represents the maximum loading capacity of OEP-Co-4OA in LNP as 5 mol%.

4. Retention of radioactive OEP-^{57}Co-OA complex in the LNPs and stability over time against aggregation in PBS

While all of the chelation, loading, and characterization studies were carried out with non-radioactive ^{59}Co, the actual formulation to be used *in vivo* had to be tested as the radioactive ^{57}Co in the OEP-Co-4OA loaded LNPs, and compared again to OEP-^{57}Co chelated cobalt without the four additional OA ligands.

4.1 OEP-^{57}Co-4OA retention in PBS and serum at 37 °C

The stability of the ^{57}Co labelling was evaluated for OEP-^{57}Co and OEP-^{57}Co-4OA loaded LNP upon incubation in PBS at 37°C and also in serum. Here, OEP-^{57}Co (2.5 µM OEP, 5.7 MBq) and OEP-^{57}Co-4OA (2.5 µM OEP, 5.7 MBq) were encapsulated in LNP (200 µM) and then incubated in PBS or serum at 37°C. As shown in **Figure 7A,** the initial encapsulation efficiency was 100% for OEP-^{57}Co-4OA (open circles) and 88% for OEP-^{57}Co (filled circles). After 1 h incubation at 37 °C the encapsulation efficiency had decreased for OEP-^{57}Co to 75%, while it was almost the same for OEP-^{57}Co-4OA (98%). After 4 h, the encapsulation efficiency was 61% for OEP-^{57}Co and still 96% for OEP-^{57}Co-4OA, and after 24 h it had dropped quit significantly to 38 % for OEP-^{57}Co while for OEP-^{57}Co-4OA it was 88%. The results shown in **Figure 7A** therefore demonstrate the positive effect of the additional OA ligands on the stability of the OEP-^{57}Co-4OA complex providing a half-life for retention in PBS of 170 h (7 days). In the absence of the axial OA ligands, the half-life for retention of ^{57}Co was only 22h, such that the amount of free ^{57}Co after 24 h incubation at 37^{o}C was measured to be 62%, which was significantly higher than the amount of free ^{57}Co measured for OEP-^{57}Co-4OA, which was only 12 %. The retention of ^{57}Co inside LNP labeled with OEP-^{57}Co-4OA was also tested in human serum (open squares). The retention followed the retention seen in PBS. Importantly, after 24 h incubation at 37^{o}C, 89% of the initial amount of ^{57}Co was retained inside the LNP. As shown later, in **Figure 9**, this retention was found to be actually much longer than the LNP circulation half-life in the blood stream and so provided enough stability for the *in vivo* studies.

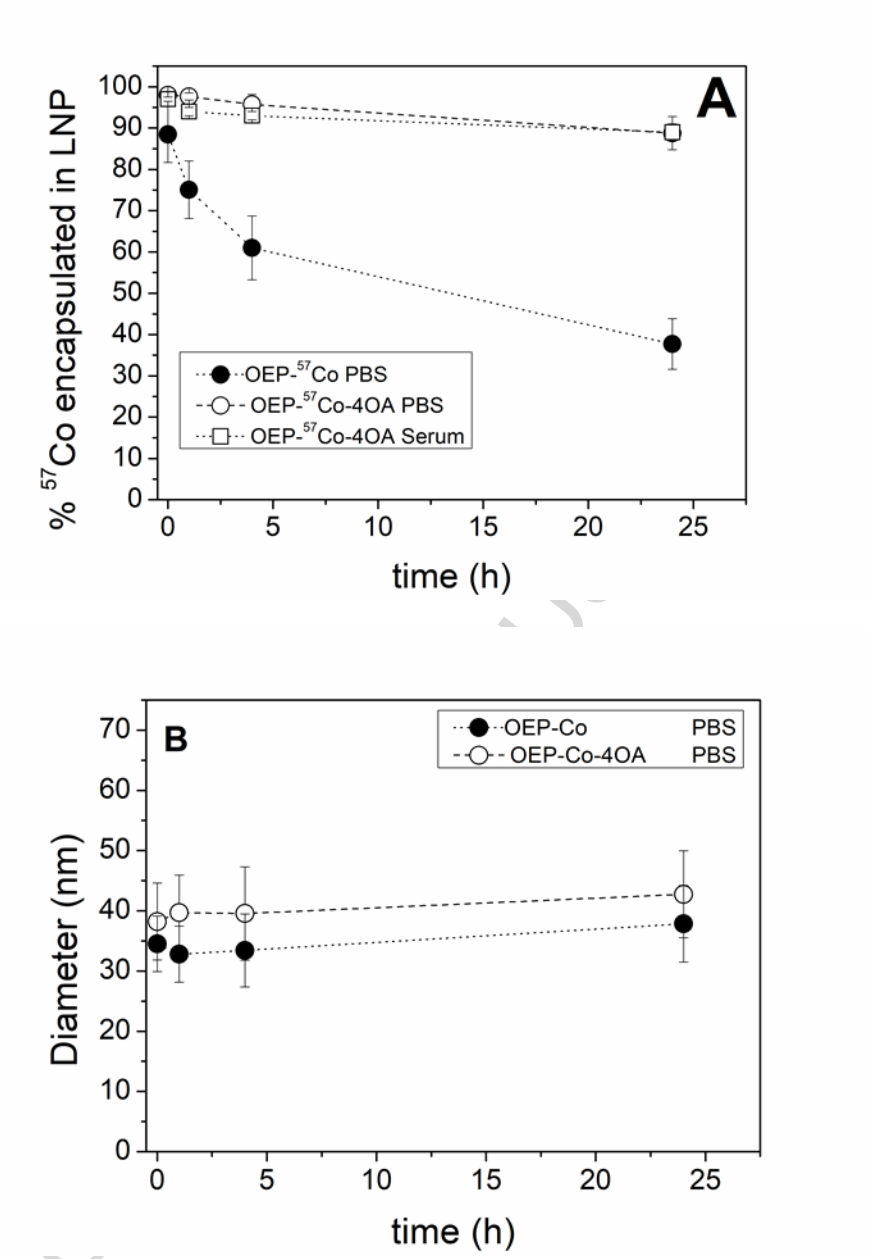

Figure 7. Co retention and LNP size stability in PBS at 37°C. A) Retention of ^{57}Co (5.7 MBq) as OEP-^{57}Co (black circle) and OEP-^{57}Co-4OA (5.7 MBq) in LNP (200 µM) upon incubation in PBS (open circle) or serum (open square)at 37°C. The half-life of the retention in OEP-^{57}Co-OA was 170h, while Co retention in OEP-^{57}Co was only 22h. The encapsulation efficacy was calculated by TLC. **B)** Time evolution of the average particle diameter for LNP (200 µM) loaded with 2.5 mol% OEP-Co (black filled circles) and OEP-Co-4OA (open circles) upon incubation in PBS at 37°C.All experiments were carried out in triplicates.

4.2 Size stability of LNP loaded with OEP-Co and OEP-Co-4OA in ionic buffer (PBS)

The size-evolution of LNP loaded with OEP-Co and OEP-Co-4OA was also measured upon incubation in PBS at 37°C (**Figure 7B**). The initial particle average diameter for OEP-Co loaded LNP was 34 ± 5 nm and for OEP-Co-4OA LNP was 38 ± 6 nm. The particle size did not change significantly during the first 4 h of incubation in PBS. However, after 24h there was a small but significant ($p<0.05$) increase of 3 nm for both OEP-Co and OEP-Co-4OA loaded LNP, to 37 nm and 41 nm respectively.

Based on these loading-, retention- and size-stability results, the complex OEP-^{57}Co-4OA was selected for labelling LNP and then used for the biodistribution study, as presented next.

5. Biodistribution study of LNP loaded with OEP-^{57}Co-4OA in tumor–bearing mice.

Finally, the *in vivo* biodistribution of LNP was studied in AR42J pancreatic tumor-bearing mice. To reiterate, after all the processing, the eventual average particle size of the injected LNP in PBS was 40±5 nm and the encapsulation efficiency of OEP-^{57}Co-4OA in the LNP was 98%. After the formulation and purification, the final LNP concentration was 2.8 mM (~4.05×10^{13} NP/mL) and the remaining activity was 90 MBq/mL in PBS suspension. Particles were diluted in PBS and 100 µL of LNP were injected i.v. at a concentration of 300 µM and radioactivity of 62 ± 4 kBq per animal. The calculated number of each injected dose of LNP was ~4.3×10^{11} particles per dose. Under these conditions, the number of ^{57}Co atoms per particle, assuming a homogenous distribution of OEP-^{57}Co-4OA amongst all LNPs, was 33 ^{57}Co atoms per LNP. The LNP biodistribution was measured 1h, 4 h and 24 h after tail vein injection. Results are shown in **Figure 8**.

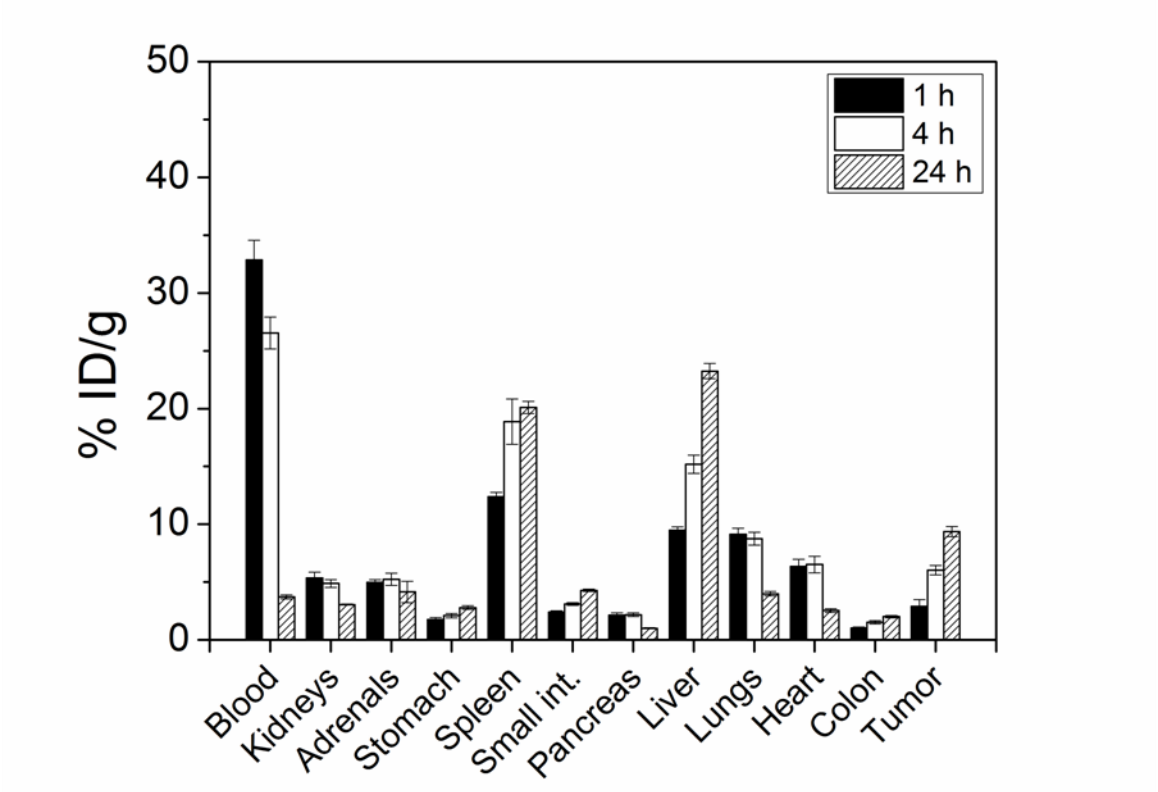

Figure 8. Biodistribution of LNP labelled with OEP-^{57}Co-4OAin mice. OEP-^{57}Co-4OA loaded LNP (62±4kBq) were injected i.v.in AR42J pancreatic tumor–bearing mice at a LNP concentration of 300 µM and the number of particles injected was $4.3x10^{11}$. The particle size of the LNP was 40 nm. The biodistribution was measured 1, 4 and 24 h after injection (mean ± SD; n=4).Tumor sizes were of a quite wide range, weighing from16-342 mg.

The concentration of LNP particles in the blood 1 h after injection was 33% ID/g, then it was decreased to 26% ID/g after 4 h and then to 4%ID/g at 24 h. As for accumulation in the various organs there was immediate uptake by the kidneys (5 %ID/g), adrenals (5 %ID/g), pancreas (2 % ID/g), lungs (9 % ID/g) and heart (6 % ID/g) at 1h, and over the 24h they each showed decreases in LNP content. There was a relatively small build up on the order of 2-4 %ID/g in other minor organs, stomach, small intestine and colon. The main organs that showed an initial major uptake were the liver and spleen. The initial liver uptake measured 1 h after injection was 9% ID/g, and increased to 23% ID/g 24 h after injection. Uptake in the spleen was also high, with 20 % ID/g measured after 24 h. The most important data was that, as shown in **Figure 8**, the tumor uptake was 3 %ID/g 1 h after particle injection and increased over time, with a particle concentration of 6 and 9 %ID/g at 4 and 24 h after injection, respectively.

Discussion

The most important result from this study was that a new method has been successfully designed and tested to formulate hydrophobic LNP so that they can contain the hydrophilic radio-diagnostic cobalt ion and are small enough (40 nm diameter) such that they can extravasate into the tumor interstitium of implanted AR42J pancreatic tumor–bearing mice. They can therefore report on the vascular permeability and the potential EPR effect for subsequent similar sized therapeutic NPs containing an anti-cancer drug [7]. Chelation of the cobalt ion was achieved by using a hydrophobic porphyrin (*OEP)* and four additional hydrophobic ligands (*OA*) at concentrations of 5 mol% with respect to the host LNP core composed of TO. Since cobalt has a preferential coordination number of six [31], by chelating it in the hydrophobic OEP and adding excess (4 equivalents) of the similarly hydrophobic OA, its octahedral geometry was stably satisfied and the cobalt was well-encapsulated and retained in the LNP. When ^{57}Co was used in this formulation, the LNP were shown to remain in blood circulation with a $t_{1/2}$ of 7.2h. Importantly, the LNP accumulated in the implanted tumors to levels of 9.4 %ID/g with a half time for accumulation of about 2h. The final 40nm average diameter LNP containing one of several radioactive cobalt isotopes is now ready for protocol optimization and preclinical studies for cobalt based imaging and therapy. For example this could include the long-lived ^{57}Co for preclinical SPECT imaging, or the positron emitting radionuclide ^{55}Co, or indeed ^{58m}Co, the Auger-electron emitting isotope with potential therapeutic applications [39, 40].

What follows next are discussions of the practical challenges solved and the significance of the data in each of the five specific aims of the project: 1. Chelate, 2. Formulate, 3. Encapsulate, 4. Retain, and 5. Measured *in vivo* biodistribution of LNP labeled with ^{57}Co in a mouse tumor model.

1. Chelation of cobalt by Octaethyl Porphyrin

The value for the association constant measured in **Figure 1B** of 2.49×10^5 $M^{-1}$was in the same range as the association constant we had measured earlier for OEP-Cu (5.44×10^5 M^{-1})[28]. This result is in agreement with the dissociation kinetics of the same complexes from porphyrins, measured albeit under acidic conditions [68]. Regarding the amount of OA required, while only 2 OAs are actually required for satisfying the additional empty chelate sites for the hexadentate Co, full chelation efficiency in the LNPs was best obtained when 4 equivalents of OA were added to OEP-Co, i.e., 2 in excess. The

efficiency of the axial coordination of amines to metalloporphyrins is higher for amines with low pKb [34], which is the case for OA (pKb of 3.3). Thus, the hexacoordinate OEP-Co could not be achieved using only OEP as chelator due to the planar symmetry of OEP, and an excess of OEP did not provide the additional axial ligands needed to get the coordination numbers higher than 4. Therefore, the hydrophobic ligand OA was used to complete the coordination sphere and to coordinate OEP-Co in the axial position (Scheme 1) since it is a hydrophobic molecule that can be retained inside LNP (log P 7.9; S_w 0.15 μM).

2. Formulation and characterization of LNP with OEP-Co-OA.

The two most important physical parameters to measure that characterize LNP for *in vitro* and *in vivo* use were the particle diameter and the surface charge expressed as the zeta potential.

2.1 Particle size

As introduced above, a particle diameter of 20 nm – 25nm is a key determinant of any NP´s ability to extravasate into the tumor interstitium (as would an LDL). It was therefore our specific aim to formulate imageable LNP with diameters at or below 40 nm and preferably on the order of 20 nm to match the size of natural LDLs and to also avoid any aggregation *in vitro* or compromised circulation *in vivo* due to protein-binding. The lipid monolayer, comprised the well-recognized stealthy composition containing 5 mol% PEG lipids (DSPE-PEG^{2000}) and was selected in order to provide for long circulation by decreasing *in vivo* uptake by the reticulo-endothelial system (RES) [69], *i.e*., mainly the liver and spleen [70, 71]. It is well know that extended circulation half-life of liposomes can also be increased by a very mechanically strong [72] and relatively impermeable [73, 74] monolayer containing cholesterol packed into the monolayer with saturated acyl chain lipids. Thus, we chose the host monolayer (that encapsulated the TO core) to be composed of DSPC:Cholesterol at a 1:1 mol ratio [69, 72], that gave the final formulation of DSPC:Cholesterol:DSPE-PEG_{2000} 45:50:5.

The size measurements showed 34±5 nm for the number-weighted average of the final formulation used in the *in vivo* tests. Studies by Walke [75] have shown that Triolein naturally precipitates out from ethanol during a rapid solvent exchange to give a size (20nm diameter nanoparticles) that is predicted by classic nucleation theory (see review by Karthika, [76]. When lipids such as palmitoyl-oleyl-phosphatidylcholine or the same DSPC-Chol-DSPE-PEG^{2000} as used here, were included, this 20nm-sized nucleate was kinetically trapped by the lipid monolayer and did not grow by aggregation,

coalescence or ripening [75]. Thus, our initial optimizations for the conditions that are required to make extravasate-able LNP came very close to this minimum size.

2.2 Zeta potential

Similarly for the zeta potential, there was actually no change in this parameter for LNP loaded with OEP-Co coordinated with different concentrations of OA (0-8 equivalents). The Z potential of LNP loaded with OEP-Co-OA was measured to be -5 mV independent of the concentration of OA (**Figure 3**). This was despite the fact that at pH 7.4 any of the OA located on the particles surface would be protonated and therefore positively charged. A negative Z potential has routinely been measured for ostensibly neutral DSPC:Cholesterol liposomes. This apparent anomaly was recently attributed to a decrease in Na^+ binding [77], leading to a similar value (-5 mV) for lipid cholesterol bilayer liposomes as in our LNP. In other work, in DSPC-coated nano-emulsions [78], it was shown that the addition of 2.5 mol% OA (compared to the phospholipid) resulted in only a very slight increase in the Z potential to positive values of just +0.13mV averaged for DSPC, DPPC and two oils, castor oil and isopropyl myristate. Our results showed the slight negative Z potentials of -5 mV for the lipid-coated particles and in the presence of excess OA. The plane of shear at which the zeta potential is measured can be as much as tens to hundreds of nm away from the surface for 5nm and 15nm NPs [79], Thus, in our case, for similarly small 30 - 40nm LNPs, it is likely that zeta potential, as an actual measurement, is less meaningful for these small nanoparticles than for larger microparticles where such measurements are used to understand the balance between van der Waals and electrostatics that are known to create force- and energy-potential balances that, in turn, stabilize or allow flocculation. In any event, for our nano-particles the most important repulsive stabilizing potential was that of the steric barrier provided by the PEG^{2000}.

3. Encapsulation of OEP-Co-OA inside LNP

As demonstrated here, in order to encapsulate the very hydrophilic ion Co^{2+} (logP = -0.57) we tested whether the octahedral OEP-Co-OA can be used to label LNP. The solubility of cobalt in water as $CoCl_2$ S_w = 4 M, based on theoretical calculations using the ALOGP method [80] (**Table 1**), is reduced $2x10^7$ fold to 0.2 µM when the ion is chelated and forms the OEP-Co-OA complex. This is expected since, as designed, the two chelators used to coordinate Co^{2+}, OEP and OA, are both very hydrophobic (OEP logP = 7.8, OA logP = 7.5), with water solubilities of S_w =16 µM, and S_w = 0.15 µM,

respectively. Taking into account that the core of LNP is composed of TO (logP =10.8; S_w = 7 nM), it is expected that OEP-Co-4OA was located within the hydrophobic core of the LNP and therefore could, in principle, affect the NP size. The effect of the OEP-Co-4OA on the particle size of the final composition of the NPs was first evaluated, followed by the quantification of the encapsulation efficiency.

3.1 Effect of encapsulating OEP-Co-4OA on NP size

As with the earlier results on OEP encapsulation (***2.1 Particle size***), the encapsulation of now OEP-Co-4OA had only a small influence over the original particle size (of 32 ± 3 nm) of LNP. As shown in **Figure 5**, at low OEP-Co-4OA concentrations (lower than 1.5 mol%) the diameter was increased only slightly and not significantly to 33 nm ($p<0.05$), while at concentrations higher than 1.5 mol% the diameter increased to 38 nm. The small dependence of particle diameter on the concentration of OEP-Co-4OA was not observed before for the OEP-Cu loaded LNP [28]. At high concentrations of OEP-Co-4OA (10 mol%) neither the particle size of LNP nor the P.I. were increased. For the free OEP-Co-4OA nanocrystal though, when measured just in buffer, their diameter was 77 nm. Thus, the size results and the low P.I. measured at high OEP-Co-4OA concentrations would suggest a good encapsulation of the complex inside LNP of up to at least 10 mol%. Thus, for the final particle, **Scheme 2** of the OEP-Co-OA loaded NPs shows the critical dimensions of the components of the LNP, i.e., the TO core and the lipid monolayer. The addition of 4OA to the formulation did not result in a significant increase in the diameter of the NPs (31nm to 40nm at a confidence of $P<0.05$) but did ensure chelation and retention of the cobalt. From x-ray diffraction it is known that the thickness of a DSPC bilayer in its liquid phase is 4.2nm [81] and that Cholesterol increases PC bilayer thicknesses by a factor of 1.2 to 5nm [82]. Thus, the lipid monolayer has a thickness of 2.5nm and PEG_{2000} extends 3.5nm [67] from the bilayer surface. This gives a total diameter for the OEP-Co-4OA LNP of 40 nm, and the hydrophobic core represents 28 nm in diameter.

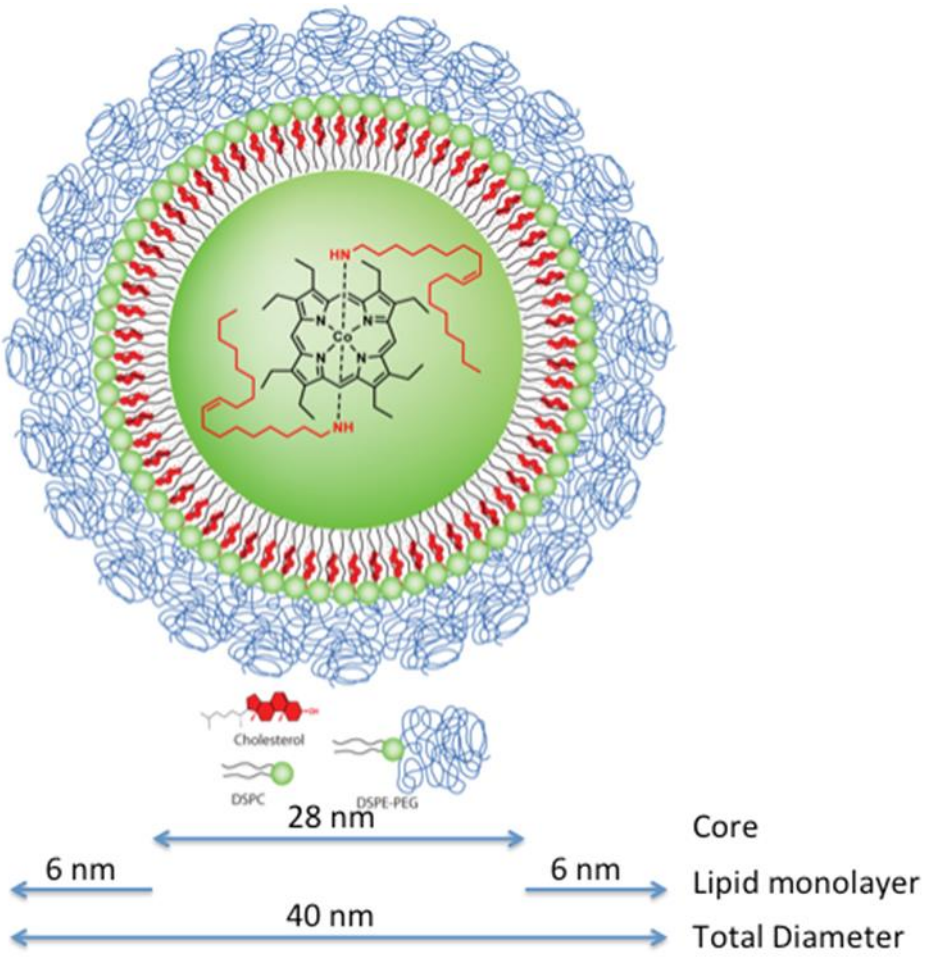

Scheme 2: Schematic representation of the OEP-Co-4OA loaded NPs prepared in this work. For a total diameter for the *OEP-Co-4OA* LNP of 40 nm, the lipid bilayer plus PEG_{2000} make up 6 nm and so the hydrophobic core represents 28 nm.

3.2 Encapsulation efficiency of Cobalt in the final LNP

When measured by fluorescent spectroscopy, the maximum OEP-Co-4OA loading inside the final LNP was actually found to be 5 mol% (**Figure 6B**). This value is consistent with our previous work where we measured a similar encapsulation efficiency of OEP and OEP-Cu inside the same LNP [28]. Here the fluorescence intensity gradually increased with increasing concentration of OEP-Co-4OA until a plateau was reached at 5 mol% concentration. Thus, if any concentration of OEP-Co-4OA above 5 mol% was in excess it was excluded from the LNPs and likely present as 77 nm nanocrystals.

4. Retention of ^{57}Co in PBS and Stability of the final LNPs against aggregation

Once incorporated, the labelling stability of LNP loaded with OEP-Co-4OA was evaluated upon incubation in PBS and human serum at 37°C for 24h, which was the time frame needed for the encapsulated ^{57}Co to inform tumor accumulation in the *in vivo* studies. From our previous results with OEP-Cu [28], the OEP-Cu complex was shown to be well-retained in the liquid core of LNP made of TO. It was therefore expected that the OEP-Co-4OA would also be well retained inside the LNP suspended in PBS and serum. Results shown in **Figure 7A** confirmed this and demonstrated the high retention of ^{57}Co in LNP when the radionuclide was chelated in the hexacoordinate OEP-^{57}Co-4OA complex. In contrast, when OA was not included in the formulation, cobalt was released from the planar tetra-coordinate OEP-^{57}Co, i.e., the cobalt retention half-life in the absence of OA from OEP-^{57}Co was only 22h. While not shown on the plot in **Figure 7A** (time axis only up to 24h) the half-life of ^{57}Co retention in OEP-^{57}Co-OA was measured to be 7 days. This result clearly proved the important role of OA to complete the preferential hexa-coordination number of cobalt in order to stabilize the ion in the chelate and LNP. While other water-soluble chelators for cobalt, such as DOTA [39, 83] or NOTA [42] can provide 6 electron donor pairs to form the stable octahedral chelate with cobalt, these chelators are too hydrophilic to be well-retained in the TO core.

Also, the size measurements for LNP labelled with OEP-Co and OEP-Co-4OA shown in **Figure 7B** demonstrated good *in vitro* stability for both LNP and showed that they are stabilized against aggregation in salt solutions and might therefore be expected to remain as individual NPs in the blood stream and so capable of crossing the leaky endothelial barrier into the tumor interstitium via the EPR effect.

5. Biodistribution Study of LNP loaded with OEP-^{57}Co-OA

Finally, the biodistribution study was carried out for LNP labelled with OEP-^{57}Co-4OA (from now identified as simply ^{57}Co-LNP). The concept was that the small NPs would be likely to follow the well-established extravasation and uptake of LDLs by tumors [84, 85] and so allow the diagnostic particle to extravasate into the tumor interstititum by the EPR effect [9, 86-88]. The results in **Figure 8** show the biodistribution profile of the ^{57}Co-LNP at 1, 4 and 24h after injection.

5.1 LNP in blood: Circulation half-life and renal excretion

The results from **Figure 7A** showed 96% of the ^{57}Co was well-retained in the ^{57}Co-LNP in PBS buffer and 94% in serum at 4 h, and so, if we assume that these data hold *in vivo*, then to a first approximation we can essentially quantify the concentration of ^{57}Co-LNP in blood by measuring the concentration of ^{57}Co. As shown in **Figure 8**, after an injected dose of $4.3x10^{11}$ ^{57}Co-LNP (injected i.v. at a concentration of 300 μM and radioactivity of 62 ± 4 kBq per animal) the concentration of ^{57}Co-LNP in the blood decreased with time from 33% ID/g at 1 h, to 27% ID/g at 4 h, and down to 4% ID/g at 24 h after injection.

This data can then be simply plotted with respect to time to provide half-lives for blood circulation and the tumor uptake rate. **Figure 9** shows the data plotted on a linear time scale and the measured data point are fitted to a first order exponential with respect to time. The blood circulation concentrations of the ^{57}Co-LNP gave an estimated half-life of 7.2h. While the half-life was calculated based on just three time points, even from this limited data set, it can be seen that, the estimated half-life of ^{57}Co-LNP of 7.2 hr is only slightly shorter than other recently made and tested PET imageable NPs. These include: similarly sized (20.6 ± 5.2 nm), negatively charged zeta potential (-6.07 ± 0.71 mV) PEGylation-free biomimetic porphyrin nanoplatform,($t_{1/2}$ 9 h) [51]; and the larger diameter, ^{64}Cu-DOTA-containing liposomes ($t_{1/2}$10 h, 96.1 ± 0.8nm diameter, zeta potential -3.8 ± 0.9 mV) [89].

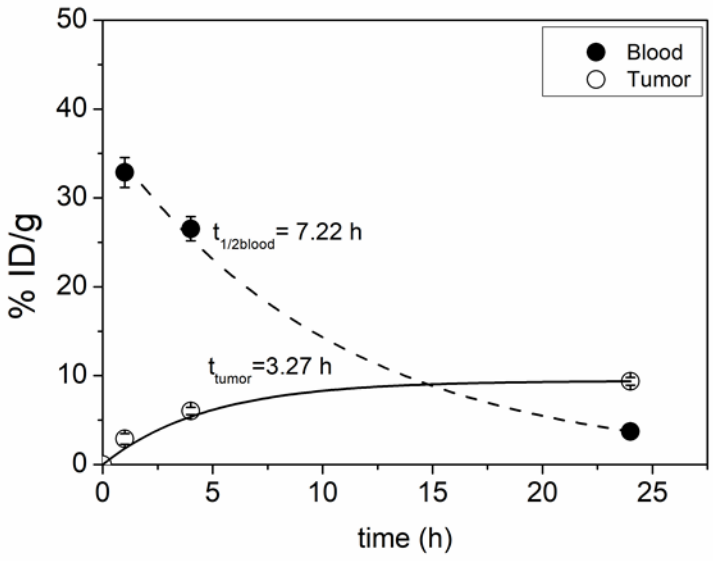

Figure 9.Plot of the %ID/g in blood and in tumor over time. The concentration of LNP loaded with OEP-^{57}Co-OA was measured in the blood (open circle) and in tumor (filled circle) 1, 4 and 24 h after injection. The experimental data was fitted to a first order kinetic decay. The half-life of ^{57}Co-LNP in blood was calculated from the fitting (dotted line) as 7.2 h. The doubling time for accumulation in the AR42J tumor (black line) was 3.27 h. The i.v. injected ^{57}Co-LNP concentration was 300 µM and the number of particles injected was $4.3x10^{11}$. The average particle size of the ^{57}Co-LNP was 40 nm.

It is therefore encouraging that there is sufficient circulation half-life in the blood stream to see good accumulation in the tumor for these sized LNP.

When compared with molecular imaging agents, such as the somatostatin receptor targeted peptide labelled with^{57}Co (^{57}Co-DOTATATE) in the same AR42J tumor model [39], ^{57}Co-LNP showed longer circulation times in the blood. As expected and desired for a molecular contrast agent, ^{57}Co-DOTATATE was already only ~0.9 % ID/g 1 h after administration and was totally cleared from the blood stream at 24 h. Hence, as it was designed to do, ^{57}Co-DOTATATE gave very little background signal even at 1h. In contrast, as required by the formulation, the chelated retention and PEGylation maintained a significant amount of the ^{57}Co-LNP in the blood stream over a significant 24h time period.

LNP has a particle size of 40 nm that is expected to be large enough to avoid renal clearance (>5nm). In fact, we observed a maximum accumulation in the kidneys of only 5 %ID/g, which could easily reflect the non-perfused blood volume of this highly vascularized organ. Interestingly our value of 5 %ID/g is similar to the values obtained for porphyrin-loaded nanoparticles reported by others [51], with 20 nm diameter. This value is however much lower than the value obtained for the molecular imaging agent ^{57}Co-DOTATATE (15%ID/g) [39], that is mainly eliminated through the kidneys, so we can conclude that the LNP are not being eliminated from circulation through the kidney but through the liver, as discussed next.

5.2 LNP accumulation in the liver

One of the most effective ways the body uses to remove foreign NPs (even beneficial ones) from the blood stream is via opsonization by blood borne clotting agents and recognition of the opsonized NP by the Kupffer cells of the liver [71]. **Figure 8** shows that the liver accumulation of our PEGylated ^{57}Co-LNP 24 h after injection was 23%ID/g. For comparison, this was similar to the liver uptake values

reported by Cui *et al*., for their non-PEGylated, porphyrin-based ultra-small nanostructures termed porphylipoprotein (PLP) with a diameter of 20 nm [51].

5.3 LNP accumulation in tumors

Finally, as mentioned above, the most important result is that the NPs could indeed accumulate in tumors up to levels that are similar to many of the NPs used recently [8]. Comparing to specific NPs tested in the same AR42J tumor model by others, Helbok et reported ^{111}In liposomes targeted with the somatostatin analogue tyrosine-3-octreotide as a tumor targeting agent [90]. NP biodistribution studies showed that only moderate tumor uptake was found in the xenografted nude mice (<2.5% ID/g) at 4 h post injection, compared to 6% ID/g for the ^{57}Co-LNPs (see **Figure 9**). The ^{57}Co-LNP tumor uptake was also much higher than for poly-lactate polymeric micelles with a much larger 100 nm diameter (2 %ID/g) again in the same tumor model of pancreatic cancer [91].

For comparison with a molecular imaging agent, the tumor uptake of ^{57}Co-LNP was, as expected, very different to ^{57}Co-DOTATATE. The ^{57}Co-LNP tumor uptake was only at about half the values reported for the somatostatin-targeted molecular agent ^{57}Co-DOTATATE [39]. As shown in **Figure 8**, and replotted in **Figure 9**, tumor accumulation of ^{57}Co-LNP increased over time, from 3%ID/g to 6 %ID/g to 9.4 %ID/g measured at 1h, 4h, and 24h respectively after injection. Thus, compared to ^{57}Co-DOTATATE, while the tumor accumulation of ^{57}Co-LNP was lower than the accumulation of ^{57}Co-DOTATATE that shows a maximum accumulation of 24%ID/g [39], ^{57}Co-LNP tumor accumulation was nevertheless, almost 50% of this molecular agent's accumulation.

We calculated a tumor-to-blood ratio of 1.6 (**Figure S2**) for ^{57}Co-LNP 24 h after injection. This value is much lower (by a factor of 75 - 85) than the values preferred and obtained for small peptides targeted to the somatostatin receptor (tumor-to-blood ratio of 121-137) [39]. This is because small molecules can extravasate into the tumor interstitium due to its small size (a few nanometers) and active targeting, resulting in a fast and high tumor accumulation and penetration of 24%ID/g 1 h after injection and a rapid and complete loss from the blood stream. The important point here is that, the LNPs were not designed to be used as a tumor-diagnostic agent in the classical sense of simply detecting metastatic tumors. Rather, they were designed to be used in the context of an individualized medicine strategy (see below, ***"PET imaging in personalized nanomedicine"***), in diagnosis and therapy using NPs that need to accumulate in the tumor interstitium. Thus, as is now clear from the biodistribution study, NPs

with a defined diameter (40nm) and surface properties (PEGylation) can accumulate at the tumor site. Information of tumor accumulation provided by the LNP can now be used to predict the expected pharmacokinetics of therapeutic NPs with the same diameter and coating composition, but now carrying a core of pure drug. Their ability to accumulate in tumors would be an essential event that would determine their potential for efficacy. As we have seen, when compared with molecular imaging agents, despite the longer circulation time and the smaller tumor uptake for the LNPs, tumor-uptake was still twice that for other LDL-sized NPs [51] or liposomes [89], albeit in different tumor models. That is, since our LNPs were designed to accumulate in the perivascular space of metastatic tumors, a half-life of 7.2 h might well be long enough to achieve the overall goal of measuring tumor permeability and to signify that sufficient NP drug could be subsequently accumulated to expect efficacy.

5.4. LNP Pharmacokinetic vs pure Cobalt

One criticism could be the absence of a free cobalt control. To this we point out that our *in vitro* data (**Figure 7. Co retention and LNP size stability in PBS at 37°C**) showed how well the Cobalt was retained in the specifically chelated Co-OEP-OA in the nanoparticle. Mainly because of this data we did not do a pure cobalt chloride control in this first study of the nanoparticles. Also, data *in vivo* in the literature for pure cobalt suggests that all our measurements did in fact reflect the behavior of the nanoparticle-encapsulated cobalt because the half-lives for its blood circulation and for liver retention are vastly different compared to those reported for pure cobalt.

For example, in Jansen's 1996 paper [10], after intravenous administration in rats, all tissues showed rapid ^{55}Co uptake, but the **liver** and **bladder** accumulated most of the ^{55}Co. In our studies we did not report the bladder content, and there is certainly a strong Cobalt-signal in the liver. However, in Jansen's study the biological half-life of free cobalt was 25.5 h, and the residence half-life in the liver was 7.5 hr. This is in sharp contrast to our study of the cobalt-retained nanoparticles where the circulation half-life of the cobalt signal was only 7.5 h and accumulation in the liver was still increasing at 24h (see **Figure 8. Biodistribution of LNP labelled with OEP-^{57}Co-4OA in mice 1, 4, and 24 hrs).** Thus, given these vastly different pharmacokinetics for free Cobalt versus our well-encapsulated, chelated cobalt, we can conclude that it is indeed the intact nanoparticles that still retain their trapped

Cobalt and not free cobalt that is giving any of these signals. It is the nanoparticle-encaspulated cobalt that is reporting nanoparticle-accumulation in the tumor.

5.5 PET imaging and Individualized anti-cancer nanomedicine

Ongoing studies in our lab and collaborators are focused on endogenous-inspired NP designs for metastatic cancer, including: synthesis, characterization, and formulation of a pro-drug Niclosamide Stearate (NSNP) for i.v. injection [6, 75]; NSNP testing for *in vitro* cell-uptake and cytotoxicity in glioblastoma, breast & prostate cancers. These prodrug nanoparticles are showing promising and positive results in *in vivo* preclinical studies in a flank and metastatic tumors with growth delays and extended lifetimes for the NSNP-treated animals [22]. However, it is essential that the EPR effect is proven and characterized in order for the therapeutics to have any chance of success. Thus, as laid out in this paper, any clinical (or preclinical) testing and use of the nanoparticle design can now include PET-imageable nanoparticles which in combination with the NSNPs forms a suite of diagnostic and therapeutic "Individualized nanomedicines" for cancer.

Measurement of the tumor accumulation of nanomedicines to predict the anti-cancer therapy is recognized as a key step in the development of "*Individualized-" or "personalized-nanomedicines"*[28, 92, 93], and that is exactly what the purely diagnostic LNPs presented here can offer. The overall concept was to provide a diagnostic (PET-imageable) and therapeutic (hydrophobic drugs [7, 75] option in two separate NPs that have different content, but are physically similar in terms of surface chemistry to enhance circulation half-life (a sterically stabilizing PEG layer) and size to promote vascular extravasation and tumor accumulation (20-40nm diameter). It is envisioned that a "personalized anti-cancer nanomedicine approach" relies on the selection of patients who are the more likely responders to a particular nanomedicine treatment. Using the fatty acid synthase inhibitor Orlistat [94] as an example, it would:

1. detect the presence of the tumors (e.g., by ^{18}FDG)
2. determine by an additional *functional imaging agent* that the tumor was susceptible to a certain drug-target pathway (e.g., ^{11}C-acetate signifying activity of fatty acid synthase),
3. quantitatively evaluate NP access to, and accumulation in, the tumor interstitium[92], by for example, a PET-imageable LNP,

4. administer the drug NP for therapy. (i.e. Orlistat nanoparticles to block the fatty acid synthase pathway).

Thus, these imageable NPs would necessarily be of the same size and physical state as the subsequent drug NP. Tumor accumulation of NPs has been quantitatively measured in preclinical studies by PET [48, 95-97] and in human patients by SPECT [12] imaging using NPs labelled with long-lived radionuclides. What has been achieved now is a method to prepare NPs with the same size and structure as the subsequent LDL-sized therapeutic nano-medicines, labelled in their hydrophobic core with a long-lived PET radionuclide that, again, physico-chemically (mainly size and surface) resembles the subsequent drug NP that would provide the therapeutic intervention.

Conclusions

The additional hydrophobic chelator OA was indeed needed to obtain a stable octahedral OEP-Co-4OA. After 24h *in vitro* incubation, ^{57}Co was actually well-retained at levels of 89% inside LNP in the OEP-^{57}Co-4OA complex, compared to the OEP-^{57}Co complex (38%), which is important for *in vivo* administration and to ensure a sufficient blood circulatory half-life. The half-life of the retention in OEP-^{57}Co-OA was 7 days, while in OEP-^{57}Co was only 22h. Because of this high retention, we could measure the circulation half-life and organ and tissue biodistribution of 40 nm diameter LNPs containing ^{57}Co, including the appearance of tumor accumulation *in vivo*. Thus, the LNP containing the OEP-Co-4OA complex, with diameters of 40nm, accumulated in pancreatic AR42J tumors of mice at concentrations of 9.4 % ID/g. The method described in the present work for the core-labelling of LNPs with cobalt is now ready for labeling of NPs with ^{55}Co, or indeed other hexadentate radionuclides of interest (including, ^{89}Zr, ^{86}Y and the Auger-emitter^{58m}Co) for preclinical *in vivo* PET-imaging and radio-therapeutics.

Acknowledgements

This work was supported by grant project nº232149 from the Danish National Research Foundation, Niels Bohr Professorship.

References

[1] A. Arslanagic, Establishing the feasibility for endogenous delivery of pure-drug anti-cancer nanoparticles in the treatment of metastatic breast cancer disease, in: Biochemistry and Molcular Biology, SDU, 2018 (exp).
[2] A. Arslanagic, P. Hervella, K. Glud, J. Mollenhauer, David Needham, Characterization of targeted and non-targeted uptake in breast cancer stem cells of triple negative origin, in: CLINAM, Basel, Switzerland, 2016.
[3] L. Karimi, Preclinical Characterization and In vitro Cell Testing of Novel Niclosamide Nanoparticle Formulations for Treatment of Prostate Cancer, in: Biochemistry and Molecular Biology, SDU, 2019 (exp).
[4] L. Karimi, P. Hervella, K. Glud, J. Mollenhauer, D. Needham, Novel Formulation of Orlistat for the Treatment of Breast Cancer, in: CLINAM, Basel, Switzerland, 2016.
[5] D.L. Kerr, H. Mikati, A. Tovmasyan, W. Chen, P. Walke, R.T. Kreulen, J. Somarelli, S.B. Dewitt, T. Camp, J. Herbert, D.S. Hsu, B. Brigman, G. Hanna, G. Palmer, D. Needham, W. Eward, A novel formulation of niclosamide treats metastatic osteosarcoma in vivo, in: Connective Tissue Oncology Society, Maui, Hawaii, 2017.
[6] P. Hervella, A. Arslanagic, P. Walke, C. Azevedo, T. Ulven, D. Needham, Formulation Characterization and in vitro cytotoxicity of Niclosamide Stearate Prodrug Nanoparticles, (in preparation), (2018).
[7] D. Needham, A. Arslanagic, K. Glud, P. Hervella, L. Karimi, P.F. Høilund-Carlsen, K. Kinoshita, J. Mollenhauer, E. Parra, A. Utoft, P. Walke, Bottom Up Design of Nanoparticles for Anti-Cancer Diapeutics:
"Put the drug in the Cancer's food", J. Drug Targeting 24 (2016) 36-856.
[8] S. Wilhelm, A.J. Tavares, Q. Dai, S. Ohta, J. Audet, H.F. Dvorak, W.C.W. Chan, Analysis of nanoparticle delivery to tumours, 1 (2016) 16014.
[9] A.D. Wong, M. Ye, M.B. Ulmschneider, P.C. Searson, Quantitative Analysis of the Enhanced Permeation and Retention (EPR) Effect, PLoS ONE, 10 (2015) e0123461.
[10] O'Brien ME, Wigler N, Inbar M, Rosso R, Grischke E, Santoro A, Catane R, Kieback DG, Tomczak P, Ackland SP, Orlandi F, Mellars L, Alland L, T. C, Reduced cardiotoxicity and comparable efficacy in a phase III trial of pegylated liposomal doxorubicin HCl (CAELYX/Doxil) versus conventional doxorubicin for first-line treatment of metastatic breast cancer, Ann Oncol., 15 (2004) 440-449.
[11] F.J. Gordon AN, Guthrie D, Parkin DE, Gore ME, Lacave AJ., Recurrent epithelial ovarian carcinoma: a randomized phase III study of pegylated liposomal doxorubicin versus topotecan., J Clin Oncol., 19 (2001) 3312-3322.
[12] K.J. Harrington, S. Mohammadtaghi, P.S. Uster, D. Glass, A.M. Peters, R.G. Vile, J.S. Stewart, Effective targeting of solid tumors in patients with locally advanced cancers by radiolabeled pegylated liposomes, Clinical cancer research : an official journal of the American Association for Cancer Research, 7 (2001) 243-254.
[13] A. Soundararajan, A. Bao, W.T. Phillips, R. Perez, B.A. Goins, (186)Re-Liposomal Doxorubicin (Doxil): In Vitro Stability, Pharmacokinetics, Imaging and Biodistribution in a Head and Neck Squamous Cell Carcinoma Xenograft Model, Nuclear medicine and biology, 36 (2009) 515-524.
[14] H. Petersen, P.C. Holdgaard, P.H. Madsen, L.M. Knudsen, D. Gad, A.E. Gravergaard, M. Rohde, C. Godballe, B.E. Engelmann, K. Bech, D. Teilmann-Jørgensen, O. Mogensen, J. Karstoft, J. Johansen, J.B. Christensen, A. Johansen, P.F. Høilund-Carlsen, FDG PET/CT in cancer: comparison of actual use with literature-based recommendations, on behalf of the, P. E. T. C. T. Task Force of the Region of Southern Denmark, European Journal of Nuclear Medicine and Molecular Imaging, 43 (2016) 695-706.
[15] P. Ziai, M.R. Hayeri, A. Salei, A. Salavati, S. Houshmand, A. Alavi, O.M. Teytelboym, Role of Optimal Quantification of FDG PET Imaging in the Clinical Practice of Radiology, RadioGraphics, 36 (2016) 481-496.
[16] I. Grassi, C. Nanni, V. Allegri, J.J. Morigi, G.C. Montini, P. Castellucci, S. Fanti, The clinical use of PET with (11)C-acetate, American Journal of Nuclear Medicine and Molecular Imaging, 2 (2012) 33-47.

[17] J. Xie, S. Lee, X. Chen, Nanoparticle-based theranostic agents, Advanced drug delivery reviews, 62 (2010) 1064-1079.
[18] S.M. Janib, A.S. Moses, J.A. MacKay, Imaging and drug delivery using theranostic nanoparticles, Advanced Drug Delivery Reviews, 62 (2010) 1052-1063.
[19] T. Lammers, S. Aime, W.E. Hennink, G. Storm, F. Kiessling, Theranostic Nanomedicine, Accounts of Chemical Research, 44 (2011) 1029-1038.
[20] S. Yue, J. Li, S.-Y. Lee, Hyeon J. Lee, T. Shao, B. Song, L. Cheng, Timothy A. Masterson, X. Liu, Timothy L. Ratliff, J.-X. Cheng, Cholesteryl Ester Accumulation Induced by PTEN Loss and PI3K/AKT Activation Underlies Human Prostate Cancer Aggressiveness, Cell Metabolism, 19 (2014) 393-406.
[21] R.A. Firestone, Low-Density Lipoprotein as a Vehicle for Targeting Antitumor Compounds to Cancer Cells, Bioconjugate Chem, 5 (1994) 105-113.
[22] D.L. Kerr, A. Tovmasyan, J. Herbert, P. Walke, J. Herbert, G. Palmer, G. Hanna, W. Eward, D. Needham, A New Prodrug Nanoparticle of Niclosamide Shows Positive Preclinical Responses in both Flank and Lung-Metastatic Tumours at doses of only 0.3mg.kg and 0.15mg/kg, respectively, (In preparation), (2018).
[23] M. Dobbelstein, U. Moll, Targeting tumour-supportive cellular machineries in anticancer drug development, Nat Rev Drug Discov, 13 (2014) 179-196.
[24] M. Narvekar, H.Y. Xue, J.Y. Eoh, H.L. Wong, Nanocarrier for Poorly Water-Soluble Anticancer Drugs—Barriers of Translation and Solutions, AAPS PharmSciTech, 15 (2014) 822-833.
[25] R. Ghadi, N. Dand, BCS class IV drugs: Highly notorious candidates for formulation development, Journal of Controlled Release, 248 (2017) 71-95.
[26] G.L. Amidon, H. Lennernäs, V.P. Shah, J.R. Crison, A Theoretical Basis for a Biopharmaceutic Drug Classification: The Correlation of in Vitro Drug Product Dissolution and in Vivo Bioavailability, Pharmaceutical Research, 12 (1995) 413-420.
[27] T. Loftsson, M.E. Brewster, Pharmaceutical applications of cyclodextrins: basic science and product development, Journal of Pharmacy and Pharmacology, 62 (2010) 1607-1621.
[28] P. Hervella, E. Parra, D. Needham, Encapsulation and retention of chelated-copper inside hydrophobic nanoparticles: Liquid cored nanoparticles show better retention than a solid core formulation, European Journal of Pharmaceutics and Biopharmaceutics, 102 (2016) 64-76.
[29] K. Kilian, M. Pęgier, K. Pyrzyńska, The fast method of Cu-porphyrin complex synthesis for potential use in positron emission tomography imaging, Spectrochimica Acta Part A: Molecular and Biomolecular Spectroscopy, 159 (2016) 123-127.
[30] Y. Zhou, K.E. Baidoo, M.W. Brechbiel, Mapping biological behaviors by application of longer-lived positron emitting radionuclides, Adv Drug Deliver Rev, 65 (2013) 1098-1111.
[31] L.r. Rulíšek, J. Vondrášek, Coordination geometries of selected transition metal ions (Co2+, Ni2+, Cu2+, Zn2+, Cd2+, and Hg2+) in metalloproteins, Journal of Inorganic Biochemistry, 71 (1998) 115-127.
[32] S. Shao, J.M. Geng, H.A. Yi, S. Gogia, S. Neelamegham, A. Jacobs, J.F. Lovell, Functionalization of cobalt porphyrin-phospholipid bilayers with his-tagged ligands and antigens, Nature Chemistry, 7 (2015) 438-446.
[33] D.C. Hodgkin, J. Kamper, M. Mackay, J. Pickworth, K.N. Trueblood, J.G. White, Structure of Vitamin B12, Nature, 178 (1956) 64-66.
[34] F.A. Walker, STERIC AND ELECTRONIC EFFECTS IN COORDINATION OF AMINES TO A COBALT(II) PORPHYRIN, Journal of the American Chemical Society, 95 (1973) 1150-1153.
[35] G. Hao, A. N Singh, W. Liu, X. Sun, PET with Non-Standard Nuclides, Current Topics in Medicinal Chemistry, 10 (2010) 1096-1112.
[36] I. Fichtner, D. Arndt, R. Reszka, J. Gens, Pharmacokinetic behavior of [57Co]bleomycin liposomes in mice: comparison with the unencapsulated substance, Anti-cancer drugs, 2 (1991) 555-563.

[37] H. Wållberg, S. Ahlgren, C. Widström, A. Orlova, Evaluation of the radiocobalt-labeled [MMA-DOTA-Cys61]-Z HER2:2395-Cys affibody molecule for targeting of HER2-expressing tumors, Molecular Imaging and Biology, 12 (2010) 54-62.
[38] A. Heppeler, J.P. Andre, I. Buschmann, X. Wang, J.C. Reubi, M. Hennig, T.A. Kaden, H.R. Maecke, Metal-ion-dependent biological properties of a chelator-derived somatostatin analogue for tumour targeting, Chemistry (Weinheim an der Bergstrasse, Germany), 14 (2008) 3026-3034.
[39] H. Thisgaard, B.B. Olsen, J.H. Dam, P. Bollen, J. Mollenhauer, P.F. Hoilund-Carlsen, Evaluation of Cobalt-Labeled Octreotide Analogs for Molecular Imaging and Auger Electron-Based Radionuclide Therapy, Journal of Nuclear Medicine, 55 (2014) 1311-1316.
[40] H. Thisgaard, M.L. Olesen, J.H. Dam, Radiosynthesis of Co-55- and Co-58m-labelled DOTATOC for positron emission tomography imaging and targeted radionuclide therapy, Journal of Labelled Compounds & Radiopharmaceuticals, 54 (2011) 758-762.
[41] J.H. Dam, B.B. Olsen, C. Baun, P.F. Hoilund-Carlsen, H. Thisgaard, In Vivo Evaluation of a Bombesin Analogue Labeled with Ga-68 and Co-55/57, Molecular imaging and biology : MIB : the official publication of the Academy of Molecular Imaging, (2015).
[42] J.H. Dam, B.B. Olsen, C. Baun, P.F. Hoilund-Carlsen, H. Thisgaard, In Vivo Evaluation of a Bombesin Analogue Labeled with Ga-68 and Co-55/57, Molecular imaging and biology : MIB : the official publication of the Academy of Molecular Imaging, 18 (2016) 368-376.
[43] B. Mitran, H. Thisgaard, Rosenstr, #xf6, U. m, J.H. Dam, M. Larhed, V. Tolmachev, A. Orlova, High Contrast PET Imaging of GRPR Expression in Prostate Cancer Using Cobalt-Labeled Bombesin Antagonist RM26, Contrast Media & Molecular Imaging, 2017 (2017) 10.
[44] T.A. Tran, D. Rosik, L. Abrahmsen, M. Sandstrom, A. Sjoberg, H. Wallberg, S. Ahlgren, A. Orlova, V. Tolmachev, Design, synthesis and biological evaluation of a multifunctional HER2-specific Affibody molecule for molecular imaging, European Journal of Nuclear Medicine and Molecular Imaging, 36 (2009) 1864-1873.
[45] J. Garousi, K.G. Andersson, J.H. Dam, B.B. Olsen, B. Mitran, A. Orlova, J. Buijs, S. Stahl, J. Lofblom, H. Thisgaard, V. Tolmachev, The use of radiocobalt as a label improves imaging of EGFR using DOTA-conjugated Affibody molecule, Scientific reports, 7 (2017) 5961.
[46] J.A. Cardarelli, D.W. Slingerland, B.A. Burrows, A. Miller, MEASUREMENT OF TOTAL-BODY COBALT-57 VITAMIN-B12 ABSORPTION WITH A GAMMA-CAMERA, Journal of Nuclear Medicine, 26 (1985) 941-943.
[47] J. Korf, L. Veenma-van der Duin, R. Brinkman-Medema, A. Niemarkt, L. de Leij, Divalent cobalt as a label to study lymphocyte distribution using PET and SPECT, Journal of Nuclear Medicine, 39 (1998) 836-841.
[48] D.W. Bartlett, H. Su, I.J. Hildebrandt, W.A. Weber, M.E. Davis, Impact of tumor-specific targeting on the biodistribution and efficacy of siRNA nanoparticles measured by multimodality in vivo imaging, Proceedings of the National Academy of Sciences of the United States of America, 104 (2007) 15549-15554.
[49] L.M. Mahakian, D.G. Farwell, H. Zhang, J.W. Seo, B. Poirier, S.P. Tinling, A.M. Afify, E.M. Haynam, D. Shaye, K.W. Ferrara, Comparison of PET Imaging with Cu-64-Liposomes and F-18-FDG in the 7,12-Dimethylbenz a anthracene (DMBA)-Induced Hamster Buccal Pouch Model of Oral Dysplasia and Squamous Cell Carcinoma, Molecular Imaging and Biology, 16 (2014) 284-292.
[50] A.L. Petersen, T. Binderup, P. Rasmussen, J.R. Henriksen, D.R. Elema, A. Kjaer, T.L. Andresen, 64Cu loaded liposomes as positron emission tomography imaging agents, Biomaterials, 32 (2011) 2334-2341.
[51] L. Cui, Q. Lin, C.S. Jin, W. Jiang, H. Huang, L. Ding, N. Muhanna, J.C. Irish, F. Wang, J. Chen, G. Zheng, A PEGylation-Free Biomimetic Porphyrin Nanoplatform for Personalized Cancer Theranostics, ACS nano, 9 (2015) 4484-4495.
[52] R. Rossin, D.P.J. Pan, K. Qi, J.L. Turner, X.K. Sun, K.L. Wooley, M.J. Welch, Cu-64-labeled folate-conjugated shell cross-linked nanoparticles for tumor imaging and radiotherapy: Synthesis, radiolabeling, and biologic evaluation, Journal of Nuclear Medicine, 46 (2005) 1210-1218.

[53] T. Schluep, J. Hwang, I.J. Hildebrandt, J. Czernin, C.H.J. Choi, C.A. Alabi, B.C. Mack, M.E. Davis, Pharmacokinetics and tumor dynamics of the nanoparticle IT-101 from PET imaging and tumor histological measurements, Proceedings of the National Academy of Sciences of the United States of America, 106 (2009) 11394-11399.
[54] H. Cai, Z. Li, C.-W. Huang, A.H. Shahinian, H. Wang, R. Park, P.S. Conti, Evaluation of Copper-64 Labeled AmBaSar Conjugated Cyclic RGD Peptide for Improved MicroPET Imaging of Integrin αvβ3 Expression, Bioconjugate Chem., 21 (2010) 1417-1424.
[55] C.A. Boswell, X. Sun, W. Niu, G.R. Weisman, E.H. Wong, A.L. Rheingold, C.J. Anderson, Comparative in Vivo Stability of Copper-64-Labeled Cross-Bridged and Conventional Tetraazamacrocyclic Complexes, J. Med. Chem., 47 (2004) 1465-1474.
[56] H. Cai, Z. Li, C.-W. Huang, A.H. Shahinian, H. Wang, R. Park, P.S. Conti, Evaluation of Copper-64 Labeled AmBaSar Conjugated Cyclic RGD Peptide for Improved MicroPET Imaging of Integrin αvβ3 Expression, Bioconjugate Chemistry, 21 (2010) 1417-1424.
[57] P. McQuade, Y.B. Miao, J. Yoo, T.P. Quinn, M.J. Welch, J.S. Lewis, Imaging of melanoma using Cu-64- and Y-86-DOTA-ReCCMSH(Arg(11)), a cyclized peptide analogue of alpha-MSH, Journal of Medicinal Chemistry, 48 (2005) 2985-2992.
[58] D. Zeng, N.S. Lee, Y. Liu, D. Zhou, C.S. Dence, K.L. Wooley, J.A. Katzenellenbogen, M.J. Welch, 64Cu Core-Labeled Nanoparticles with High Specific Activity via Metal-Free Click Chemistry, ACS nano, 6 (2012) 5209-5219.
[59] P. van Hoogevest, A. Wendel, The use of natural and synthetic phospholipids as pharmaceutical excipients Eur. J. Lipid Sci. Technol., 116 (2014).
[60] A. Naik, R. Rubbiani, G. Gasser, B. Spingler, Visible-Light-Induced Annihilation of Tumor Cells with Platinum–Porphyrin Conjugates, Angewandte Chemie International Edition, 53 (2014) 6938-6941.
[61] A. Garai, I. Pant, S. Banerjee, B. Banik, P. Kondaiah, A.R. Chakravarty, Photorelease and Cellular Delivery of Mitocurcumin from Its Cytotoxic Cobalt(III) Complex in Visible Light, Inorganic Chemistry, 55 (2016) 6027-6035.
[62] H.M.L. Jansen, S. Knollema, L.V. van der Duin, A.T.M. Willemsen, A. Wiersma, E.J.F. Franssen, F.G.M. Russel, J. Korf, A.M.J. Paans, Pharmacokinetics and Dosimetry of Cobalt-55 and Cobalt-57, Journal of Nuclear Medicine, 37 (1996) 2082-2086.
[63] E. Parra, P. Hervella, D. Needham, Real-Time Visualization of the Precipitation and Phase Behavior of Octaethylporphyrin in Lipid Microparticles, Journal of Pharmaceutical Sciences, 106 (2016) 1025-1041.
[64] L. Flamigni, A.M. Talarico, B. Ventura, A practical approach to the study of photoactive self-assembled porphyrin systems, Journal of Porphyrins and Phthalocyanines, 07 (2003) 318-327.
[65] C.D. Tait, D. Holten, M. Gouterman, PICOSECOND PHOTOLYSIS OF AXIAL LIGANDS ON COBALT(II) AND COBALT(III) PORPHYRINS, Journal of the American Chemical Society, 106 (1984) 6653-6659.
[66] T. Teerlink, Peter G. Scheffer, Stephan J. L. Bakker, and Robert J. Heine, Combined data from LDL composition and size measurement are compatible with a discoid particle shape, Journal of Lipid Research, 45 (2004) 954-966.
[67] A.K. Kenworthy, K. Hristova, D. Needham, T.J. McIntosh, Range and magnitude of the steric pressure between bilayers containing phospholipids with covalently attached poly(ethylene glycol), Biophysical Journal, 68 (1995) 1921-1936.
[68] E.M. Kuvshinova, D.L. Kuz'min, N.S. Dudkina, S.G. Pukhovskaya, A.S. Semeikin, O.A. Golubchikov, Dissociation kinetics of copper and cobalt complexes with sterically distorted porphyrins, Russian Journal of General Chemistry, 72 (2002) 133-136.
[69] D.D. Lasic, D. Needham, The ''Stealth'' liposome: A prototypical biomaterial, Chemical Reviews, 95 (1995) 2601-2628.
[70] A. Gabizon, H. Shmeeda, Y. Barenholz, Pharmacokinetics of Pegylated Liposomal Doxorubicin, Clinical Pharmacokinetics, 42 (2003) 419-436.

[71] S.M. Moghimi, A.C. Hunter, J.C. Murray, Long-circulating and target-specific nanoparticles: Theory to practice, Pharmacol. Rev., 53 (2001) 283-318.
[72] D. Needham, R.S. Nunn, ELASTIC-DEFORMATION AND FAILURE OF LIPID BILAYER-MEMBRANES CONTAINING CHOLESTEROL, Biophysical Journal, 58 (1990) 997-1009.
[73] M. Bloom, E. Evans, O.G. Mouritsen, PHYSICAL-PROPERTIES OF THE FLUID LIPID-BILAYER COMPONENT OF CELL-MEMBRANES - A PERSPECTIVE, Quarterly Reviews of Biophysics, 24 (1991) 293-397.
[74] K. Olbrich, W. Rawicz, D. Needham, E. Evans, Water permeability and mechanical strength of polyunsaturated lipid bilayers, Biophysical Journal, 79 (2000) 321-327.
[75] P. Walke, Physicochemical properties and applications of micro and nanoparticle drugs, in: Physics, Chemistry, Pharmacy, University Southern Denmark, to be submitted October 2017, 2017.
[76] S. Karthika, T.K. Radhakrishnan, P. Kalaichelvi, A Review of Classical and Nonclassical Nucleation Theories, Crystal Growth & Design, 16 (2016) 6663-6681.
[77] A. Magarkar, V. Dhawan, P. Kallinteri, T. Viitala, M. Elmowafy, T. Róg, A. Bunker, Cholesterol level affects surface charge of lipid membranes in saline solution, Scientific Reports, 4 (2014) 5005.
[78] D.F. Argenta, C.B. de Mattos, F.D. Misturini, L.S. Koester, V.L. Bassani, C.M. Simoes, H.F. Teixeira, Factorial design applied to the optimization of lipid composition of topical antiherpetic nanoemulsions containing isoflavone genistein, Int J Nanomedicine, 9 (2014) 4737-4747.
[79] H. Yu, Y. He, P. Li, S. Li, T. Zhang, E. Rodriguez-Pin, S. Du, C. Wang, S. Cheng, C.W. Bielawski, S.L. Bryant, C. Huh, Flow enhancement of water-based nanoparticle dispersion through microscale sedimentary rocks, 5 (2015) 8702.
[80] A.K. Ghose, V.N. Viswanadhan, J.J. Wendoloski, Prediction of hydrophobic (lipophilic) properties of small organic molecules using fragmental methods: An analysis of ALOGP and CLOGP methods, Journal of Physical Chemistry A, 102 (1998) 3762-3772.
[81] N. Kučerka, M.-P. Nieh, J. Katsaras, Fluid phase lipid areas and bilayer thicknesses of commonly used phosphatidylcholines as a function of temperature, Biochimica et Biophysica Acta (BBA) - Biomembranes, 1808 (2011) 2761-2771.
[82] F. de Meyer, B. Smit, Effect of cholesterol on the structure of a phospholipid bilayer, PNAS, 106 (2009) 3654-3658.
[83] T. Mastren, B.V. Marquez, D.E. Sultan, E. Bollinger, P. Eisenbeis, T. Voller, S.E. Lapi, Cyclotron Production of High-Specific Activity Co-55 and In Vivo Evaluation of the Stability of Co-55 Metal-Chelate-Peptide Complexes, Molecular Imaging, 14 (2015) 526-533.
[84] S. Vitols, G. Gahrton, A. Ost, C. Peterson, Elevated low density lipoprotein receptor activity in leukemic cells with monocytic differentiation, 1984.
[85] S. Vitols, C. Peterson, O. Larsson, P. Holm, B. Åberg, Elevated Uptake of Low Density Lipoproteins by Human Lung Cancer Tissue in Vivo, Cancer Research, 52 (1992) 6244-6247.
[86] H. Cabral, Y. Matsumoto, K. Mizuno, Q. Chen, M. Murakami, M. Kimura, Y. Terada, M.R. Kano, K. Miyazono, M. Uesaka, N. Nishiyama, K. Kataoka, Accumulation of sub-100 nm polymeric micelles in poorly permeable tumours depends on size, Nature nanotechnology, 6 (2011) 815-823.
[87] U. Prabhakar, H. Maeda, R.K. Jain, E.M. Sevick-Muraca, W. Zamboni, O.C. Farokhzad, S.T. Barry, A. Gabizon, P. Grodzinski, D.C. Blakey, Challenges and Key Considerations of the Enhanced Permeability and Retention Effect for Nanomedicine Drug Delivery in Oncology, Cancer Research, 73 (2013) 2412-2417.
[88] J. Wang, W. Mao, L.L. Lock, J. Tang, M. Sui, W. Sun, H. Cui, D. Xu, Y. Shen, The Role of Micelle Size in Tumor Accumulation, Penetration, and Treatment, Acs Nano, 9 (2015) 7195-7206.
[89] A.L. Petersen, T. Binderup, R.I. Jolck, P. Rasmussen, J.R. Henriksen, A.K. Pfeifer, A. Kjaer, T.L. Andresen, Positron emission tomography evaluation of somatostatin receptor targeted Cu-64-TATE-liposomes in a human neuroendocrine carcinoma mouse model, Journal of Controlled Release, 160 (2012) 254-263.

[90] A. Helbok, C. Rangger, E. von Guggenberg, M. Saba-Lepek, T. Radolf, G. Thurner, F. Andreae, R. Prassl, C. Decristoforo, Targeting properties of peptide-modified radiolabeled liposomal nanoparticles, Nanomedicine: Nanotechnology, Biology and Medicine, 8 (2012) 112-118.
[91] T. Miller, S. Breyer, G. van Colen, W. Mier, U. Haberkorn, S. Geissler, S. Voss, M. Weigandt, A. Goepferich, Premature drug release of polymeric micelles and its effects on tumor targeting, International Journal of Pharmaceutics, 445 (2013) 117-124.
[92] T. Lammers, L.Y. Rizzo, G. Storm, F. Kiessling, Personalized Nanomedicine, Clinical Cancer Research, 18 (2012) 4889-4894.
[93] C. Perez-Medina, D. Abdel-Atti, J. Tang, Y. Zhao, Z.A. Fayad, J.S. Lewis, W.J.M. Mulder, T. Reiner, Nanoreporter PET predicts the efficacy of anti-cancer nanotherapy, Nat Commun, 7 (2016).
[94] S.J. Kridel, F. Axelrod, N. Rozenkrantz, J.W. Smith, Orlistat Is a Novel Inhibitor of Fatty Acid Synthase with Antitumor Activity, Cancer Research, 64 (2004) 2070-2075.
[95] M.K. Danquah, X.A. Zhang, R.I. Mahato, Extravasation of polymeric nanomedicines across tumor vasculature, Advanced Drug Delivery Reviews, 63 (2011) 623-639.
[96] M.J. Welch, C.J. Hawker, K.L. Wooley, The Advantages of Nanoparticles for PET, Journal of Nuclear Medicine, 50 (2009) 1743-1746.
[97] J.W. Seo, J. Ang, L.M. Mahakian, S. Tam, B. Fite, E.S. Ingham, J. Beyer, J. Forsayeth, K.S. Bankiewicz, T. Xu, K.W. Ferrara, Self-assembled 20-nm Cu-64-micelles enhance accumulation in rat glioblastoma, Journal of Controlled Release, 220 (2015) 51-60.

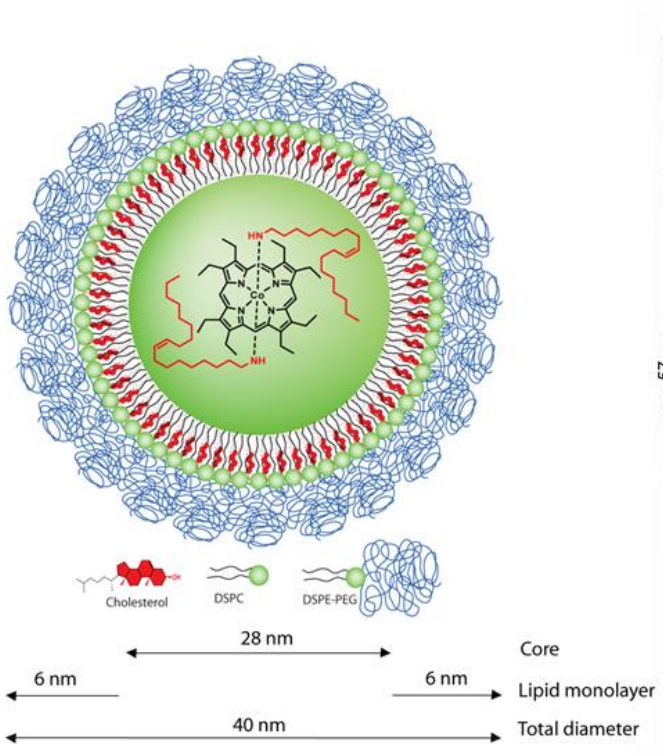

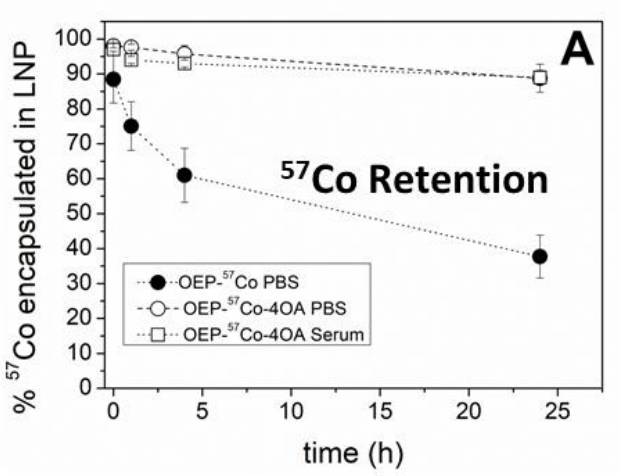

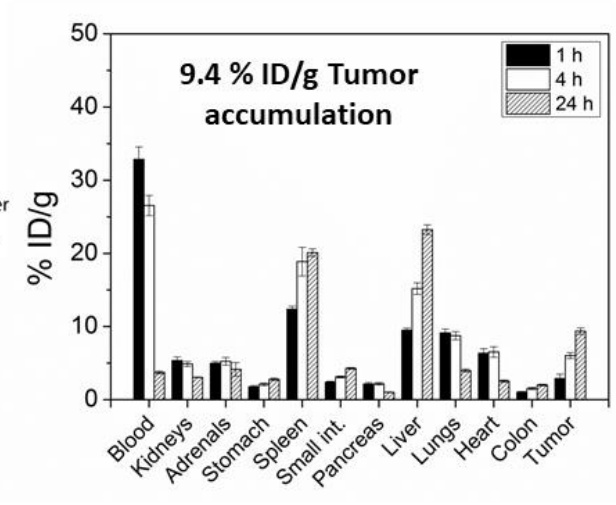

^{57}Co- Hydrophobic Liquid Nanoparticles

Graphical Abstract